Surv Geophys (2010) 31:247–283
DOI 10.1007/s10712-009-9089-8

Geophysical Signatures of Microbial Activity at Hydrocarbon Contaminated Sites: A Review

Estella A. Atekwana · Eliot A. Atekwana

Received: 10 February 2009 / Accepted: 12 October 2009 / Published online: 4 November 2009

Abstract Microorganisms participate in a variety of geologic processes that alter the chemical and physical properties of their environment. Understanding the geophysical signatures of microbial activity in the environment has resulted in the development of a new sub-discipline in geophysics called "biogeophysics". This review focuses primarily on literature pertaining to biogeophysical signatures of sites contaminated by light non-aqueous phase liquids (LNAPL), as these sites provide ideal laboratories for investigating microbial-geophysical relationships. We discuss the spatial distribution and partitioning of LNAPL into different phases because the physical, chemical, and biological alteration of LNAPL and the subsequent impact to the contaminated environment is in large part due to its distribution. We examine the geophysical responses at contaminated sites over short time frames of weeks to several years when the alteration of the LNAPL by microbial activity has not occurred to a significant extent, and over the long-term of several years to decades, when significant microbial degradation of the LNAPL has occurred. A review of the literature suggests that microbial processes profoundly alter the contaminated environment causing marked changes in the petrophysical properties, mineralogy, solute concentration of pore fluids, and temperature. A variety of geophysical techniques such as electrical resistivity, induced polarization, electromagnetic induction, ground penetrating radar, and self potential are capable of defining the contaminated zones because of the new physical properties imparted by microbial processes. The changes in the physical properties of the contaminated environment vary spatially because microbial processes are controlled by the spatial distribution of the contaminant. Geophysical studies must consider the spatial variations in the physical properties during survey design, data analysis, and interpretation. Geophysical data interpretation from surveys conducted at LNAPL-contaminated sites without a microbial and geochemical context may lead to ambiguous conclusions.

Keywords Biogeophysics · Bacteria · Biodegradation · LNAPL contamination · Geophysical methods

E. A. Atekwana (✉) · E. A. Atekwana
Boone Pickens School of Geology, 105 Noble Research Center, Oklahoma State University, Stillwater, OK 74078, USA
e-mail: estella.atekwana@okstate.edu

1 Introduction

Microorganisms participate in a wide variety of geologic processes that alter the chemical and physical properties of their environment. Microbial induced changes in rock properties have significant ramifications for near-surface geophysical investigations conducted at depths of < 100 m where microbial communities are abundant and biological processes are most active. Hydrocarbon (e.g., light non-aqueous phase liquids (LNAPL)) contaminated sites provide an ideal laboratory for investigating links between microbial processes and changes in geophysical properties. The excess organic carbon from LNAPL contamination stimulates microbial activity, leading to significant alterations of the petrophysical properties and thus changes to the geophysical signatures of the contaminated environment. Early geophysical studies that reported higher bulk electrical conductivity and attenuated ground penetrating radar (GPR) signals at LNAPL-contaminated sites were linked to microbial activity associated with biodegradation (e.g., Benson et al. 1997; Sauck et al. 1998). A large volume of literature now exists supporting the early findings of anomalous geophysical signatures at LNAPL contaminated sites undergoing bioremediation (e.g., Atekwana et al. 2000, 2002; Atekwana et al. 2004a, b, c, d; Abdel Aal et al. 2006; Bradford 2007; Cassidy 2007, 2008; Allen et al. 2007). Attempts to understand the role of microorganisms in altering the physical properties of geologic systems has resulted in the development of a new sub-discipline in geophysics called "biogeophysics" (Atekwana et al. 2006). Biogeophysics has since expanded beyond the initial hydrocarbon studies to encompass the fundamental understanding of the geophysical response of microbial interactions with geologic media, such as: biomineralization/metal cycling studies (e.g., Ntarlagiannis et al. 2005a; Williams et al. 2005; Carlut et al. 2007; Slater et al. 2007; Personna et al. 2008), growth and development of biofilms (Davis et al. 2006; Ntarlagiannis and Ferguson 2009), direct detection of microbial cells (Ntarlagiannis et al. 2005b), microbial sorption and transport in porous media (Abdel Aal et al. 2009), redox processes (Naudet and Revil 2005; Ntarlagiannis et al. 2007; Williams et al. 2007), and biogeochemical transformations of heavy metals and radionuclides (Hubbard et al. 2008).

Numerous studies have been published on the broad topic of biogeophysics; however, we focus primarily on LNAPL contamination in this review. We examine the geophysical signatures of LNAPL contamination that result from microbial processes and provide example case studies that illustrate and capture the physical changes in the contaminated environment. Every contaminated site is inherently different; thus, the LNAPL concentration, its distribution (both vertically and longitudinally) and the bio-physicochemical changes in the contaminated region (relative to the background) govern the geophysical properties. We have found that maximum changes in geophysical signatures occur in the transition, capillary, and upper portion of the saturation zones. It is within these zones that the highest populations of oil degrading microorganisms occur and the maximum changes in geophysical properties are observed.

Subsurface contamination by LNAPLs is a worldwide problem and remains one of the most widespread and prevalent sources of groundwater contamination. In the United States, more sites are contaminated by petroleum hydrocarbons than any other type of contaminant (Eweis et al. 1998). LNAPL contamination invariably leads to a complex environment and direct characterization by chemical and biological techniques that are intrusive (e.g., use of boreholes) have inherent limitations. These limitations which include the need for high density spatial coverage and high frequency of temporal sampling can be costly and time intensive. Geophysical techniques, with the advantage of rapid deployment, ability to cover spatially extensive areas at higher density, and the ability to be

deployed at higher temporal frequency, can complement biological and geochemical studies at contaminated sites.

Over the past two decades, geophysical techniques have been employed at several LNAPL contaminated sites to characterize both the spatial (e.g., Benson and Stubben 1995; Bermejo et al. 1997; Sauck et al. 1998; Atekwana et al. 2000; 2002; 2004a; Osella et al. 2002; Werkema et al. 2003; Tezkan et al. 2005; Abdel Aal et al. 2006; Sogade et al. 2006; Bradford 2007; Cassidy 2007) and temporal (e.g., Lopes de Castro and Branco 2003; Che-Alota et al. 2009) extent to understand the evolution of the contamination in the subsurface. Many of these geophysical studies have provided valuable insights into the behavior of LNAPL contamination; however, the results remain mixed. The application of the same geophysical technique at different sites, and even at different locations on the same site can produce dramatically different results. This is primarily due to the fact that the spatial and temporal characteristics of the contamination have an important bearing on the geophysical attributes and must be considered for proper interpretation.

2 Factors Governing the Detection of Subsurface LNAPL Contamination by Geophysical Techniques

The near subsurface is generally described as a porous medium and divided into a water saturated zone below the water table and a vadose zone above the water table (Fig. 1). The interface between the saturated and vadose zones contains the capillary fringe and transition zones. The capillary fringe is a tension saturation zone above the water table and can vary in thickness (being greater for finer grained material). The transition zone is a zone of

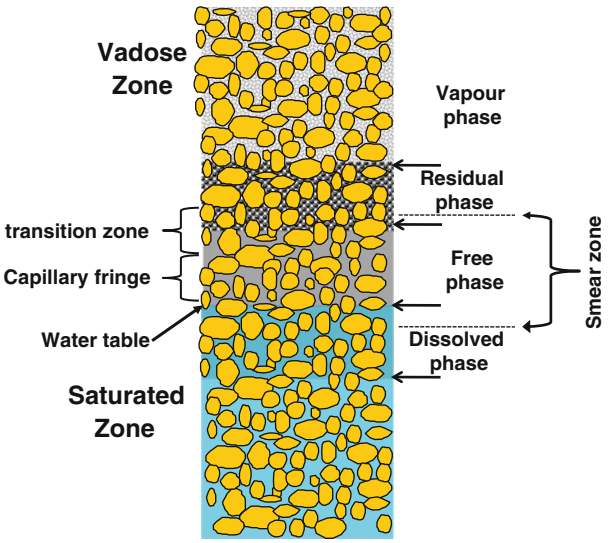

Fig. 1 Schematic of the typical distribution of soil moisture and the different phases of light non-aqueous phase liquids (LNAPLs) in the subsurface from a spill. Shortly after the spill, the LNAPL partitions into a vapour phase in the upper vadose zone, a residual phase and a free phase above the water table, and a dissolved phase in the saturated zone. Over a long time frame, fluctuating water table causes the free phase LNAPL to move up and down with the water table, causing free phase LNAPL to be trapped in isolated pockets in the saturated zone and in the region of residual phase forming a smear zone

variable saturation above the capillary fringe with decreasing water content with increasing distance above the capillary fringe. For a portion of an aquifer of similar rock/sediment matrix, the physical and chemical properties of the saturating fluids (water, contaminant, or air) control the geophysical signatures. This in turn determines which geophysical technique is able to image the subsurface physical properties.

During and shortly (weeks to several years) after a spill, the LNAPL that percolates into the subsurface partially displaces air and water in the formation. LNAPL is denser than air and, therefore, displaces the air in the vadose zone. Due to its lower density than water, LNAPL will float on water and will partially displace water and air in the capillary fringe and transition zone. LNAPL contamination is often partitioned into four distinct phases: a vapor phase, a residual phase, a free phase, and the dissolved phase (Fig. 1). Sauck (2000) provides an overview of the distribution of LNAPLs in the subsurface (Fig. 1; Sauck 2000) which has been summarized in Table form by Lopes de Castro and Branco (2003). The vapor phase consists of the volatile fractions of the hydrocarbon and is typically found in the upper parts of the vadose zone above the residual and free phase hydrocarbon zones. The vapor phase is usually limited to regions where volatilization can occur from LNAPL in the residual and free phase. The residual phase consists of LNAPL within the vadose zone that is in residual saturation and does not drain under the influence of gravity. It is limited to the source zone, but may extend beyond the source zone where the free phase LNAPL rises into the vadose zone and coats sediments due to fluctuating water table. The free phase (immiscible phase) in the capillary fringe region (which may also extend below the water table) can range in thickness from a few centimeters to several metres. The free phase can also extend laterally for several tens to hundreds of metres depending on the volume of LNAPL spillage (Fig. 2a, b, profile A–A′). Within the capillary fringe region, the LNAPL is rarely a continuous 100% free phase, but typically has <50% hydrocarbon saturation, and is mixed with air, vapor, and water (Sauck 2000). The dissolved phase occurs in the saturated zone. The concentration of the LNAPL in the aqueous phase is determined by the solubility of the different fractions which are typically low. Hence, when compared to the free phase, the total petroleum hydrocarbon concentration in the saturated zone is much lower [e.g., the solubility of benzene in water at 20°C is typically <0.1% by weight and decreases with decreasing temperature (e.g., Lucius et al. 1992)].

With time and seasonal recharge, the residual and free phase LNAPL zones move up and down in the aquifer with fluctuations in the water table. Free LNAPL is trapped in the residual zone and the upper portion of the saturated zone causing a distinct smear zone (Sauck 2000; Lee et al. 2001; Marcak and Golebiowski 2008). The lower part of the smear zone below the average water table contains an immobile residual LNAPL phase that was created by the movement of the free product into this zone during low water table conditions. The smear zone can be several metres in thickness depending on the initial thickness of the free phase LNAPL and the extent of seasonal water table fluctuations. In one study, the smear zone was estimated at ~120-cm thick for a free phase LNAPL thickness of ~30 cm (Werkema et al. 2003). Smearing also produces complexities in the LNAPL distribution causing changes in the saturation and concentration and resulting in isolated tongues or disaggregated blobs of free phase LNAPL.

The relative saturation of the different phases of the hydrocarbon varies both laterally and vertically and over time at any specific location. With time and advective transport, a LNAPL plume develops that spreads downgradient from the source area under the influence of the groundwater hydraulic gradient (Fig. 2b, profile A–A′). Within the source zone where the initial spillage occurred, both the vadose and saturated zones will be impacted by all four phases of the LNAPL (e.g., Fig. 2c, profile B–B′). Further downgradient along the longitudinal axis, the LNAPL contamination is characterized by a dissolved phase plume

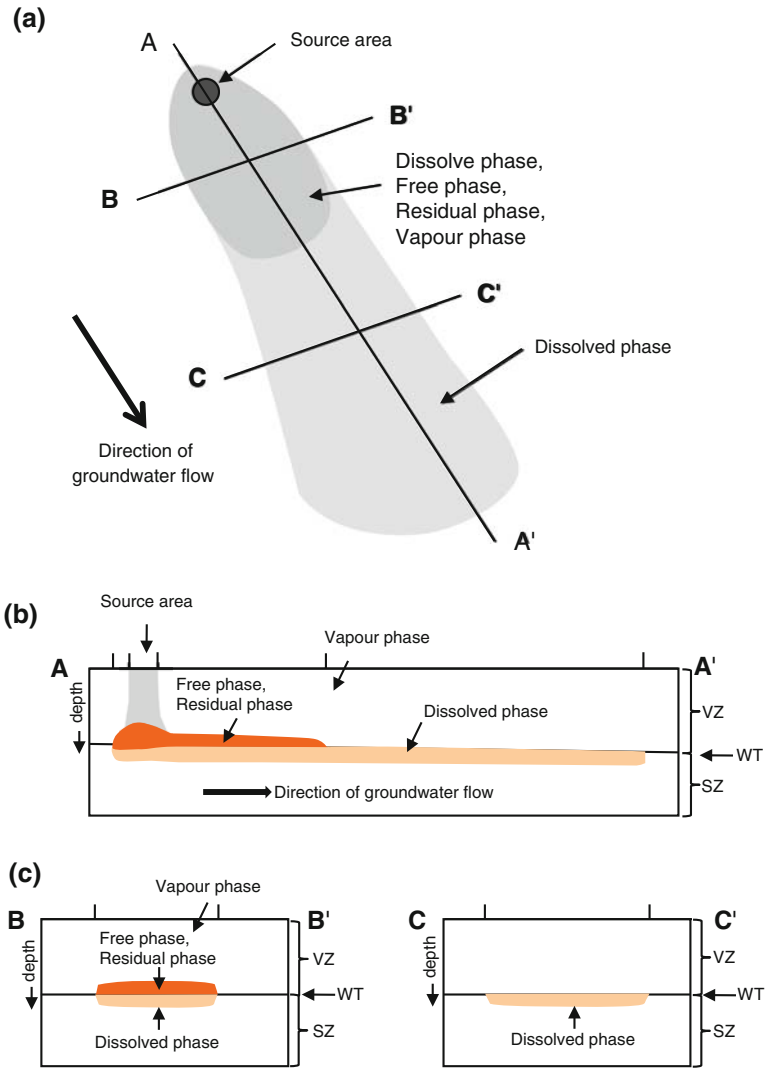

Fig. 2 Schematic of **a** plan view **b** a longitudinal cross-sectional profile, and **c** vertical cross-sectional profiles of a light non-aqueous phase liquid (LNAPL) spill. The positions of the vertical and transverse profiles are shown in (**a**). The distribution of the vapour, residual, free, and dissolved LNAPL phases are shown in each panel. VZ is the vadose zone, WT is the water table, and SZ is the saturated zone. The direction of groundwater flow is shown by *arrows* in (**a**) and (**b**). Groundwater flow is *perpendicular* to the page in (**c**)

(e.g., Fig 2c, profile C–C′). Thus, the initial and temporal distribution, relative saturation, and connectivity of the LNAPL phases at the pore scale are important for its geophysical detection (e.g., Endres and Redman 1996).

The LNAPL contaminated subsurface is a dynamic and complex bio-physicochemical environment and its geophysical response will depend on factors such as: the type of the LNAPL (crude oil, jet fuel, diesel fuel), LNAPL release history (e.g., continuous release or single release), the distribution of the LNAPL relative to air in the vadose zone or water in the saturated zone, hydrologic processes (e.g., advective transport, seasonal recharge), the

saturation history of the contaminated media, biological processes, etc. Hence, the successful application of any geophysical technique at LNAPL contaminated sites must be guided by a proper understanding of the factors that govern the geophysical responses and which of the factors are likely to dominate the geophysical responses.

3 Short-Term Geophysical Properties of Sites Contaminated by LNAPLs

By short-term, we describe a time frame weeks to several years over which chemical and biological alteration of LNAPL in the contaminated zone is negligible and only the physical separation of the LNAPL into the different phases has occurred. In this instance, the short term geophysical response of the contaminated zone is controlled by the initial concentration of LNAPL relative to air in the vadose zone and water in the capillary fringe and saturated zone. Electrical resistivity, electromagnetic induction, and GPR are some of the most common geophysical techniques employed to investigate unaltered LNAPL contamination. These techniques take advantage of the perturbations of the electrical resistivity (or bulk electrical conductivity) and permittivity of the contaminated region by the LNAPL. LNAPL is an insulator ($\sim$0.001 mS/m) relative to formation fluids ($\sim$0.1–1 mS/m for freshwater), and has low relative permittivity ($\sim$2–3) compared to clean water ($\sim$80) and water saturated sands (20–30). The replacement of pore water and air in the contaminated zone by LNAPL components will result in changes in the dc or static conductivity and relative permittivity. This would explain why early investigations of LNAPL contamination clearly show decreased electrical conductivity (Mazác et al. 1990; DeRyck et al. 1993; Lien and Enfield 1998) and enhanced GPR reflections (e.g., Daniels et al. 1995; Campbell et al. 1996; Lopes de Castro and Branco 2003) based on the insulating properties of LNAPL.

Figure 3 shows the classic resistive response of fresh LNAPL spillage in a study conducted by DeRyck et al. (1993). In this controlled spill experiment, 343 litres of kerosene were injected over a period of 33 days into a polyethylene tank filled with Borden sands, which is medium-grained sand with a porosity of 40%. The tank sediments simulated an aquifer with the top of the saturation zone at a depth of 110 cm below the surface and a capillary fringe approximately 30 cm thick. The injection of the kerosene was monitored using vertical electrical resistivity probes deployed in the sands. After the kerosene injection, decrease in water saturation in the capillary fringe (70–110 cm depth) by $\sim$17% was directly related to kerosene replacing water. The decrease in water saturation was accompanied by an increase in the electrical resistivity from $\sim$200 to $\sim$750 Ωm (Fig. 3). Increases in the electrical resistivity (from 1,100–1,200 Ωm) are also observed in the simulated upper vadose zone (e.g., 10 cm depth). However, the increases are not as large as the electrical resistivity increases observed within the capillary fringe. It is possible that the increase in resistivity in the upper vadose zone may be related to vapor effects, although this is not discussed by DeRyck et al. (1993). Yang et al. (2007) investigated a field site where a fresh LNAPL contamination resulted from an accidental underground pipeline leak in 1997. The LNAPL flooded a rice field in Nankan County in Northwest Taiwan. The authors observed much higher resistivity values of $>$140 Ωm in the contaminated compared to $<$140 Ωm in the uncontaminated regions.

Experiments conducted by Campbell et al. (1996) demonstrate the GPR response of early time spills (Fig. 4). Campbell et al. (1996) reported enhanced (brighter), higher amplitude GPR reflections in the region underneath a spill (Fig. 4 at 20–25 ns) during a controlled gasoline spill experiment at a test facility at the Oregon Graduate Institute. The brightness of the GPR reflections increased with increased pooling of the gasoline (hours 048–132;

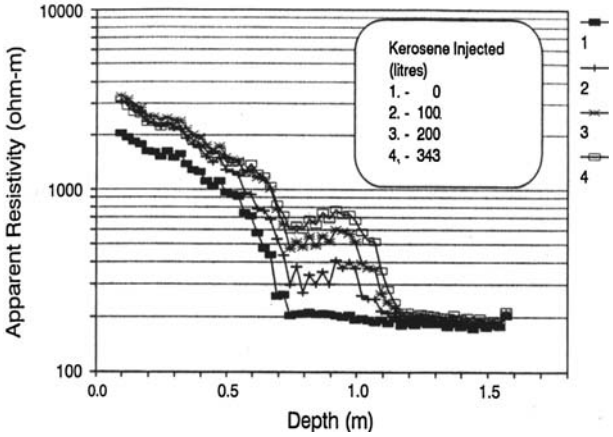

Fig. 3 Plot of bulk electrical resistivity versus depth from a controlled kerosene spill in sands. The bulk electrical resistivity for different amounts of kerosene spilled is shown. A high resistivity layer between 70 and 110 cm is due to kerosene accumulation in the capillary fringe. The water table is located at 110 cm (adapted from DeRyck et al. 1993)

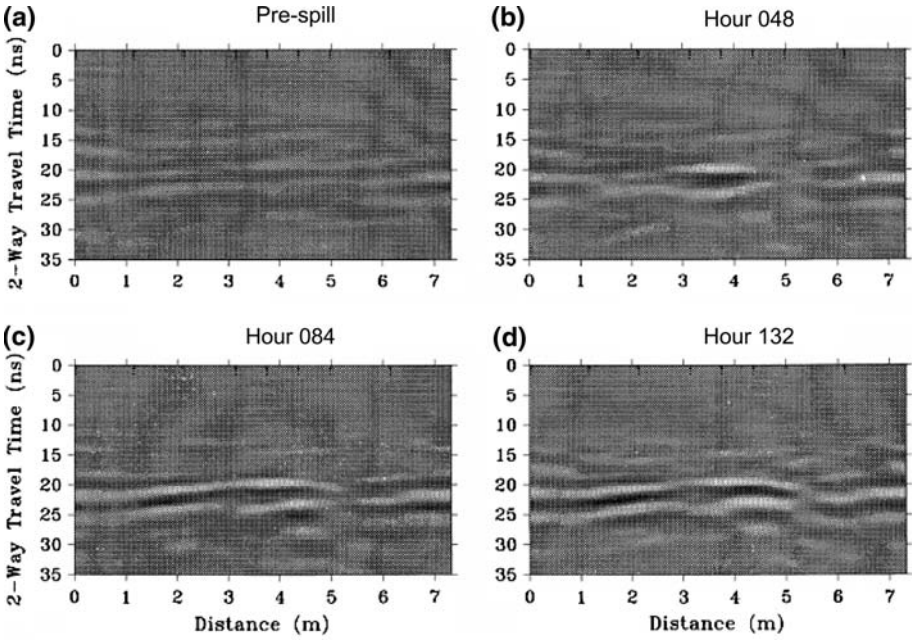

Fig. 4 **a–d** Temporal GPR profiles from a controlled gasoline spill showing bright reflections (20–25 ns) associated with the pooling of the gasoline at the water table interface. Increasing amounts of gasoline pooling over time increase the brightness of the GPR reflections (adapted from Campbell et al. 1996)

Fig. 4b, c, and d) compared to pre-spill conditions (Fig. 4a). Campbell et al. (1996) suggest that the replacement of water with a relatively high dielectric permittivity of ~ 80 by gasoline with a relatively low dielectric permittivity of ~ 2 resulted in a high velocity GPR

layer concomitant with the bright spots. Incidentally, DeRyck et al. (1993) also reported similar GPR reflection characteristics in their kerosene injection experiment.

Figure 5 shows an example of how the distribution of different phases of the LNAPL at a contaminated site results in varied GPR responses (Lopes de Castro and Branco 2003). This investigation was conducted over a gasoline spill site in Foraleza, Brazil, where gasoline leakage was first reported from an underground storage tank in 1998. The GPR surveys were initially conducted in 2001 and the site was monitored periodically over a 15 month period during a pump and treat remediation program. The GPR data were acquired using a GSSI SIR-2000 system with 900, 400, 200, and 80 MHz antennas. The 400 and 200 MHz antennas gave the best results in terms of spatial resolution and depth (e.g., Fig. 5), whilst the shallow water table ($\sim$2.67 m) provided excellent conditions for GPR. The 400 MHz data (Fig. 5a) shows a gross picture of the contaminated zone while the 200 MHz (Fig. 5b) data shows greater details of the near surface structure (vadose zone and top of saturated zone). Both antennas imaged down to 5 m (80 ns). Within the contaminated vadose zone (between 10 and 22 m horizontal distance and 2.5 m depth), a region of attenuated GPR reflections (low reflectivity) is related to the vapor phase, whereas enhanced reflections are associated with the free and residual phases located directly above the water table. A high reflectivity zone below the water table (2.67 m; Fig. 5) is related to the dissolved phase LNAPL.

The complexity of the subsurface spatial distribution of different LNAPL phases is also illustrated in a GPR-based study by Cassidy (2008). In this study, Cassidy (2008) shows that LNAPL geometries within the contaminated smear zone greatly affect the frequency component of the GPR response and exhibit distinct spectral responses. Models in the Cassidy (2008) study present likely scenarios of LNAPL distribution encountered in a smear zone and include: (1) a uniform mixture of pore fluids (LNAPL/pore water mixtures of different percentages), (2) small-scale disaggregated LNAPL units (consisting of randomly

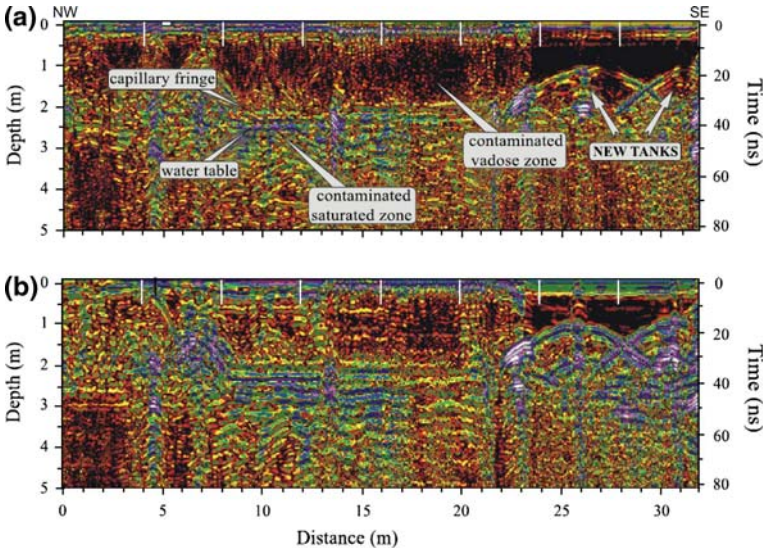

Fig. 5 Ground penetrating radar (GPR) profiles from a hydrocarbon contaminated site acquired at **a** 400 MHz and **b** 200 MHz showing how the different phases of light non-aqueous phase liquid (LNAPL) result in varied GPR responses. Both panels show different GPR response in the contaminated vadose zone, capillary fringe, and saturated zone (adapted from Lopes de Castro and Branco 2003)

distributed disaggregated blobs of fully saturated LNAPLs within a background of contaminated water), (3) large pools of spatially distinct free phase LNAPLs (thick LNAPL lenses), and (4) a large number of thin LNAPL lenses and a small number of thin LNAPL lenses (Fig. 2; Cassidy 2008). The Cassidy (2008) study illustrates that the GPR response varies both as a result of the distribution of the various phases of LNAPL as well as the macro and pore scale distribution of the LNAPL.

In summary, laboratory and field studies of the geophysical response of LNAPL spills over the short-term show that the geophysical characteristics of the contaminated environment is due largely to the contrast in the physical properties of the LNAPL and the aquifer. This is primarily due to the fact that fresh LNAPL spills have not been significantly altered or weathered by chemical or biological processes.

4 Long-Term Geophysical Properties of Sites Contaminated by LNAPLs

4.1 The Role of Bacteria

The geophysical properties of LNAPL-contaminated sites over long time periods of several years to decades are related to the extent of physical, chemical, and biological alteration of LNAPL. This time frame has been described qualitatively as "aged hydrocarbon" (Atekwana et al. 2000), implying that considerable time and sufficient alteration by environmental and biologic processes is required for the contaminated region to develop physical properties that sufficiently contrast with the background and region contaminated by unaltered LNAPL. The degree to which alterations will occur depend on the environmental conditions as determined by subsurface geology, temperature, moisture content, and microbial activity.

Similar to landfills, LNAPL-contaminated environments are akin to bioreactors. The excess organic carbon serves as an electron donor, accelerating biological activity that degrades the LNAPL. During microbial oxidation of organic compounds, electrons are transferred to terminal electron acceptors (TEAs) (O_2, NO_3^-, Fe(III), Mn(IV), SO_4^{2-}, CO_2) through coupled redox reactions (e.g., Huling et al. 2002). While biodegradation is typically correlated with the sequential utilization of TEAs, the distribution of terminal electrons is highly dynamic and exhibits spatiotemporal variations (Vroblesky and Chapelle 1994) that are driven by the changing hydrologic conditions. It is well documented that LNAPL contamination can cause significant changes in bacterial diversity and shifts in microbial populations even in extreme environments such as Antarctic soils (e.g., Saul et al. 2005). Efficient biodegradation is largely controlled by the presence of microbial populations capable of degrading the specific LNAPLs in question and the occurrence of favorable geochemical and hydrological conditions for biodegradation to occur (Haack and Bekins 2000).

Microbes are ubiquitous in the subsurface and indigenous microbes rapidly adapt to the use of excess carbon from LNAPL contamination. Microbial processes can cause significant changes in the contaminated aquifer, the aquifer matrix, and the water bearing capacity of the aquifers (Chapelle and Bradley 1997). The growth and proliferation of microbes alter the hydraulic properties (e.g., hydraulic conductivity) of the aquifer (e.g., Vandevivere and Baveye 1992; Brovelli et al. 2009), and microbial metabolism and production of waste alter the ionic composition of groundwater and pore fluids. The changes in groundwater and pore fluid chemical composition will depend on the nature of electron donor and electron acceptor processes and the extent of microbial alteration of the LNAPL.

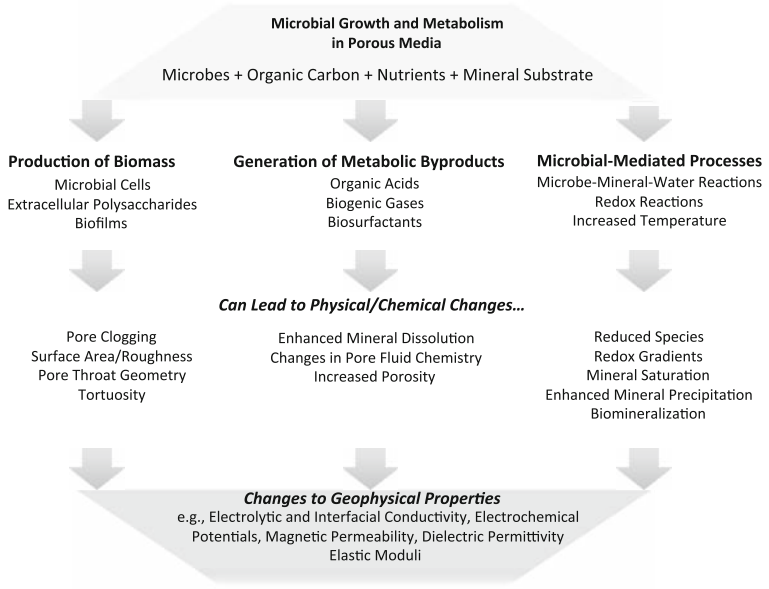

Fig. 6 Generalized conceptual diagram showing that microbial growth and activity in porous media can alter the physicochemical properties, and, thus, the geophysical signatures (from C. Davis, unpublished)

Microbial alteration of aquifer properties result in changes in the geophysical properties due to one or more of the following (Fig. 6):

1. an increase in oil-degrading microbial populations over time,
2. attachment of the microbes on mineral surfaces and the development of biofilms,
3. clogging of aquifer pores by microbial cells and by biofilms,
4. the decrease in the concentration of the LNAPL from microbial utilization of carbon,
5. production of metabolic byproducts during microbial degradation of the LNAPL such as organic acids, biosurfactants, and biogenic gases (e.g., CO_2, H_2S, CH_4, H_2),
6. alteration of mineral surfaces due to weathering enhanced by either direct action of colonized bacteria and/or by the byproducts (e.g., carbonic and organic acids) of degradation,
7. increases in the solute concentration from mineral weathering and changes in the saturation state of solutes in the groundwater and pore fluids,
8. precipitation of biomaterials or different mineral phases (resulting from the byproducts of the microbial metabolism) on mineral surfaces and in pores, and
9. TEA processes which cause sequential decreases and increases in solute species and change the redox chemistry of the groundwater and pore water.

4.2 Bio-Induced Alterations of the Petrophysical Properties in LNAPL Contaminated Environments

In order to discuss the effects of microbial activity on physical properties of the contaminated environment, we provide a brief background on electrical resistivity (ER)/induced polarization (IP), electromagnetic induction (EM), GPR, and self potential (SP)

techniques, as these have commonly been used to investigate LNAPL contamination in field settings. More extensive discussions on petrophysical properties can be found in the geophysics literature (e.g., Schön 1996).

4.2.1 Electrical Resistivity and Induced Polarization Methods

Archie's equation has been used to analyze the electrical resistivity responses of fluid-filled porous rocks (Archie 1942) and demonstrates a fundamental quantitative relationship between the bulk formation resistivity (ρ_b), pore water resistivity (ρ_w), porosity (ϕ), and the degree of saturation (S_n):

$$\rho_b = a\rho_w\phi^{-m}S^{-n} \tag{1}$$

where a (a dimensionless parameter related to the grain shape), m (a dimensionless parameter commonly referred to as the cementation exponent), and n (the saturation exponent) are material constants and empirically derived. Archie's formula is considered to be valid for medium- to coarse-grained sediments where the grain surface conductivity (reciprocal of resistivity) does not contribute to the bulk electrical conduction. Equation 1 is frequently used to estimate hydrocarbon saturation in 'clean' sandstones and other relatively permeable reservoir rocks in the oil industry. The contribution of grain surface conduction becomes significant when small grain sizes dominate the lithology and/or when clay minerals are present. In this case, Archie's formula is modified to include the contribution of the grain surface resistivity (ρ_s) (Waxman and Smits 1968):

$$\frac{1}{\rho_b} = \frac{\phi^m}{a\rho_w}S^n + \frac{1}{\rho_s} \tag{2}$$

The presence of microbial cell with large surface areas, their attachment to mineral surfaces, and alteration of their host environment can contribute to the grain surface resistivity (e.g., Atekwana et al. 2004b; Abdel Aal et al. 2004).

DC resistivity methods are responsive to both electrolyte and solid–fluid interface (surface) chemistry, but are unable to differentiate between the relative contributions of electrolytic verses interface conductivity. The IP method, in particular the complex conductivity method, is an extension of the dc-resistivity method (e.g., Olhoeft 1985) whereby the conductivity magnitude and phase response are measured and used to calculate the real and imaginary conductivity. The sensitivity of the IP method to subtle changes in the surface chemical properties of mineral grains make IP ideal for investigating the effect of bio-physicochemical changes on the electrical properties due to microbial activity (Abdel Aal et al. 2004, 2006). Traditionally, the IP method has been predominantly used to investigate disseminated sulfide ores and to a lesser extent in groundwater exploration. However, in the last decade, IP techniques have increasingly been used in environmental applications to map contaminant plumes and for salt water intrusion studies (e.g., Slater and Lesmes 2002; Sogade et al. 2006). IP measurements are sensitive to the low-frequency capacitative properties of rocks and sediments that result from diffusion controlled polarization processes at the interface between mineral grains and the pore fluid. These polarization mechanisms are responsive to changes in the lithology and pore fluid chemistry (Slater and Lesmes 2002), and the direct presence of microbial cells (Abdel Aal et al. 2004, 2009; Ntarlagiannis et al. 2005b; Davis et al. 2006).

The in-phase (real; σ') conductivity component of complex conductivity represents ohmic conduction currents (energy loss) and is sensitive to changes in fluid chemistry,

whereas the out-of-phase (imaginary; σ'') component represents the much smaller polarization (energy storage) term which is sensitive to physicochemical properties at fluid-grain interface (Schön 1996; Revil and Glover 1998; Lesmes and Frye 2001). The measured magnitude ($|\sigma|$) and phase (ϕ) parameters are related to the real and imaginary components as follows:

$$|\sigma| = \sqrt{(\sigma'^2 + \sigma''^2)} \tag{3}$$

$$\phi = \tan^{-1}\left[\frac{\sigma''}{\sigma'}\right] \cong \left[\frac{\sigma''}{\sigma'}\right] \quad (\phi < 100\,\text{mRads}). \tag{4}$$

The real (σ') and imaginary (σ'') components of the complex conductivity are calculated by:

$$\sigma' = |\sigma| \cos\,\phi \tag{5}$$

$$\sigma'' = |\sigma| \sin\,\phi \tag{6}$$

Conduction and polarization at the grain-fluid interface are a function of surface area, surface charge density, surface ionic mobility, and interfacial geometry. IP measurements in unconsolidated sediments and sandstones show a positive correlation with surface area (Börner and Schön 1991; Schön 1996) and an inverse correlation with grain size (Schön 1996; Slater and Lesmes 2002; Slater and Glaser 2003). IP responses are generally attributed to two physical mechanisms: electrode or metallic polarization (occurs at a metal/fluid interface and is of a larger magnitude) and membrane polarization which occurs at a non-metal/fluid interface (e.g., in the presence of clay particles or by constriction of pores) and is of a smaller magnitude.

4.2.2 Electromagnetic Methods (EM)

Electromagnetic induction methods are some of the most common EM techniques applied to environmental investigations such as contaminant plume mapping. These methods involve the propagation of continuous wave or transient electromagnetic fields in and over the Earth associated with alternating currents induced in the subsurface by a primary field. The source of energy for the EM method is introduced into the ground by direct contact or inductive coupling through a coil or long wire placed on the ground. An advantage of the EM method over the electrical resistivity method is that it does not require direct contact with the ground; hence, airborne surveys can be conducted. Furthermore, variations in the EM properties with depth can easily be obtained by using different frequencies.

Most EM surveys at LNAPL contaminated sites typically involve the use of ground conductivity meters. An excellent review of ground conductivity meters can be found in McNeill (1990) and only a limited presentation is made here. Ground conductivity meters are horizontal loop electromagnetic (HLEM) systems commonly used in mining exploration. However, they are different from the traditional HLEM systems in that the operating frequency is low enough that electrical skin depth is significantly greater than the intercoil spacing. Therefore, virtually all the response is in the quadrature phase of the received signal. The zero level of the quadrature component is accurately set such that readings are direct measure of ground conductivity down to the estimated depth of penetration. The instruments make use of the induction number defined as the ratio of the intercoil spacing r to the skin depth d. With these constraints, the secondary magnetic field can be represented as:

$$\frac{H_s}{H_p} = \frac{i\mu_o \sigma \omega r^2}{4} \tag{7}$$

where H_s is the secondary magnetic field at the receiver coil, H_p is the primary magnetic field at the receiver coil, ω is the angular frequency ($2\pi f$), μ_0 is the permeability of free space, σ is the ground conductivity in S/m, r is the intercoil spacing in metres, and $i = (-1)^{1/2}$, denoting that the secondary field is 90° out of phase with the primary field. Measured parameters include the apparent conductivity in millisiemens per metre (mS/m) and the in-phase ratio of the secondary to primary magnetic field in parts per thousand (ppt).

Another EM technique that has been applied to hydrocarbon plume mapping and for exploration of the shallow subsurface is the radiomagnetotelluric method (RMT). An explanation of the principles of this technique can be found in Tezkan et al. (2005) and much of their discussion on the RMT method is excerpted here. The RMT-method is a relatively new EM technique that uses EM waves produced by high powered civilian and military transmitters operating at frequencies between 10 and 300 kHz. At great distances from the transmitters, the EM fields can be assumed to be due to a plane wave. The EM field consists of two components: a horizontal magnetic field component (H_y) perpendicular to the direction of propagation and a horizontal electric field (E_x) in the direction of propagation (Eq. 8). Any anomalous conductivity body in the Earth will modify the measured magnetic and electric fields (Tezkan et al. 2005). The ratio of the orthogonal electric and magnetic horizontal components for the observed frequencies is related to the apparent resistivity of the subsurface. Thus, the measured parameters of the RMT technique are similar to those of the magnetotelluric method (Cagniard 1953). Hence, the apparent resistivity (ρ_a) and phase values (ϕ) can be calculated for selected frequencies from the measured magnetic and electric field values using the Cagniard equation (Cagniard 1953):

$$\rho_a = \frac{1}{2\pi f \mu_0}\left|\frac{E_x}{H_y}\right|^2, \quad \phi = \tan^{-1}\left[\frac{\mathrm{Im}\,(\mathrm{E_x}/\mathrm{H_y})}{\mathrm{Re}\,(E_x/H_y)}\right] \tag{8}$$

where E_x and H_y denote the electric and magnetic field, μ_0 the permeability of the free space, and f the selected frequency.

In both the EM and RMT techniques, conductivity is the primary physical property of investigation. Because conductivity is the inverse of resistivity, the factors that affect resistivity will also affect conductivity measurements, hence Archie's Law (Eq. 1) also applies to EM surveying (in this case the Archie parameters are expressed in terms of conductivity). Because oil is an insulator, hydrocarbon contamination will decrease the bulk electrical conductivity of the subsurface. However, the effects of biodegradation as discussed in Sect. 4.3 are likely to cause increases in the bulk electrical conductivity. For example, an increase in total dissolved solids from the weathering of aquifer materials by organic acids produced by microbes during biodegradation is likely to cause an increase in the pore water conductivity and, hence, the bulk electrical conductivity of the contaminated media.

4.2.3 GPR Method

The GPR method is another electromagnetic technique that is routinely applied at LNAPL-contaminated sites and differs from resistivity and IP in that it is a high frequency electromagnetic method that is analogous to seismic reflection techniques. The higher

frequencies result in higher spatial resolution when compared to the ER/IP techniques; however, the depth of investigation is also limited. The EM wave velocity (v) is given by:

$$v = \frac{1}{\sqrt{\mu\varepsilon}} \tag{9}$$

where μ is the magnetic permeability and ε is the dielectric permittivity. It is often assumed that magnetic permeability μ does not vary significantly and, hence, the dielectric permittivity ε is the physical property that generally determines the EM wave velocity in geological materials. ε is a measure of electric charge polarization that occurs when an electric field is applied to a medium. Commonly the dielectric behavior is characterized in terms of the relative dielectric permittivity κ (also known as the dielectric constant):

$$\kappa = \frac{\varepsilon}{\varepsilon_o} \tag{10}$$

where ε_0 is the permittivity of a vacuum (8.8542×10^{-12} F/m). Using κ and neglecting the effects of μ (near surface sediments and soils are often considered to be non-magnetic), the EM wave velocity is then given by:

$$v = \frac{c}{\sqrt{\kappa}} \tag{11}$$

where c is the velocity of light in a vacuum (0.3 m/ns). Water has a significantly higher κ (80) than other commonly occurring geological materials (κ for dry sand and gravel is $\sim$4–10 and for NAPLs $\sim$2), hence, GPR techniques commonly provide information on water content (saturation) (Davis and Annan 1989). Attenuation and depth of penetration of the GPR signals depend on the electrical conductivity (σ) and the dielectric permittivity (ε) of the medium:

$$\alpha \approx \frac{\sigma}{2}\sqrt{\mu/\varepsilon} \tag{12}$$

α is the attenuation constant in dB/m and σ is the conductivity. High values of σ result in a highly attenuative medium. Thus, in Eqs. 9 and 10, the dielectric permittivity controls the radar velocity, while the electrical conductivity controls the attenuation (Knight 2001). As a result, GPR works well in dry, clay-free conditions such as sand and gravel.

Microbial degradation causes changes in the chemical and physical properties of the contaminated media which can change the dielectric permittivity. For example, from Eq. 12, changes in pore fluid conductivity of the aquifer caused by microbial activity will impact the attenuation constant α. Also the precipitation of magnetic minerals resulting from biotransformation of iron related minerals within the contaminated environment may likely increase the magnetic permeability, potentially impacting GPR measurements, since the magnetic permeability is an important parameter that governs the propagation of GPR waves (Eq. 9). However, in most GPR investigations, the magnetic permeability is ignored since it is often assumed that for most sediments the magnetic permeability does not vary significantly. We suggest that, in the interpretation and modeling of GPR signals from microbially altered environments, the effects of enhanced magnetic permeability should be considered.

4.2.4 Self Potential Method

The SP technique is a passive electrical geophysics method based on measurements of naturally occurring electric potentials generated by internal electrical current sources. This

potential is typically measured using non-polarizable electrodes (e.g., $Cu/CuSO_4$ or $Pb/PbCl_2$) in contact with the ground surface (or down borehole) with respect to a reference electrode that is usually fixed and at some distance away from the target of interest. The two electrodes are typically connected via a wire to a high input impedance (>100 MΩ) voltmeter. A more detailed description of this technique can be found in Corwin (1990), Bigalke and Grabner (1997), and Nyquist and Corry (2002). The naturally occurring potentials arise from three main mechanisms: streaming potential, diffusion potential, and mineralization potential. The streaming potential also known as electrokinetic or electrofiltration potential is associated with the flow of water in porous media (Rizzo et al. 2004). This potential is thought to be due to the coupling between the fluid ions and bound charges on the solid capillary walls as shown below:

$$E_s = \frac{\rho \varepsilon \zeta \Delta P}{4\pi\eta} \tag{13}$$

ρ is the fluid electric resistivity, ε is the fluid dielectric permittivity, η is the fluid dynamic viscosity, ζ is the zeta potential, and ΔP is the pressure difference.

The diffusion potentials are electro-diffusional effects associated with gradients in the chemical potentials of the ionic charge carriers (Linde and Revil 2007). Local variations in electrolytic concentration cause potential differences due to the difference in anion and cation mobilities in solutions of differing concentration.

$$E_d = \frac{-RT(I_a - I_c)}{nF \ln(C_1/C_2)} \tag{14}$$

R is the gas constant (8.31 J/°C), F is the Faraday's constant (9.65×10^4 C/mol), T is the absolute temperature (K), n is the electric charge/ion, I_a and I_c are the mobility of anions and cations, and C_1 and C_2 are the solution concentrations creating the diffusion gradient.

Mineralization potentials are SP anomalies associated with mineral ore deposits and are typically the target for exploration. The mineralization potentials result from redox reactions and coupled electron transport associated with electronic conductors such as metallic ore deposits (geobattery model of Sato and Mooney 1960; Sivenas and Beales 1982; Stoll et al. 1995). Other SP sources include thermoelectric (resulting from temperature gradients and are the important SP sources for geothermal exploration) and bioelectric potentials [due to the action of ion selectivity and water pumping action of plant roots (e.g., Nyquist and Corry 2002)]. Both the streaming and diffusion potentials typically produce small anomalies in the range of tens of millivolts. Only the geobattery mechanism resulting from mineral potentials is known to produce potentials in the hundreds of millivolts range. In the natural environment the SP response often results from a combination of the above mechanisms.

In the past, the SP method was mostly used for mineral, oil, and geothermal exploration. However, SP has received greater attention for its potential application to environmental and hydrogeologic problems due to its sensitivity to groundwater flow and redox chemistry (e.g., Nyquist and Corry 2002; Naudet et al. 2003; Rizzo et al. 2004). Microbial degradation of organic carbon can cause significant changes in both the groundwater redox chemistry and dissolved solute concentrations resulting in measurable large SP anomalies (>100 mV). We note that while the SP source mechanism resulting in mineralization potentials is largely accepted (the geobattery model of Sato and Mooney (1960) where the ore body serves as an electronic conductor bridging two different redox zones), the mechanism generating SP anomalies at organic rich contaminated sites is still not well understood, and the role of bacteria remains a subject of much controversy.

4.3 Conceptual Model of Bio-Induced Changes in Petrophysical Properties of LNAPL Contaminated Environments

Figure 6 is a generalized conceptual model illustrating how microbial activity can alter the petrophysical properties of porous media by causing changes in the matrix character (e.g., surface area/surface roughness) and chemistry of the pore fluids. Microbial cell growth and the attachment of biofilms to mineral grain surfaces and as colonies within pores (left side of Fig. 6) will cause changes in the pore characteristics such as size and tortousity (pore-volume changes). Pore constriction will enhance membrane polarization effects (e.g., Ntarlagiannis et al. 2005b). Changes in the pore volume can also occur by microbial mediated processes (right side of Fig. 6) whereby, conductive mineral phases such as iron hydroxides and clays or insulating phases such as calcite precipitate in pore spaces and reduce porosity and permeability, and, hence, hydraulic conductivity. The deposition of conductive mineral phases will increase the bulk electrical conductivity (Eq. 1), as well as lead to an enhancement of the surface conductivity (Eq. 2) (e.g., Slater et al. 2007). Furthermore, the presence of conductive mineral phases may cause attenuation of the GPR signal amplitude (Eq. 12).

The dissolution of minerals by metabolic byproducts such as organic and carbonic acids can increase the pore fluid electrical conductivity and enhance porosity (middle of Fig. 6). Figure 7a is a scanning electron microscope (SEM) image of a mineral grain obtained from a LNAPL contaminated site which shows etched pits and a remarkable pattern of dissolution features. The dissolution features suggest intense mineral surface alteration by the microbial processes. Figure 7b is a SEM image of a mineral grain also obtained from a LNAPL contaminated site which shows bacteria in a biofilm attached to a mineral surface. This is evidence that implicates microbes in the alteration of the surfaces of the mineral grains. The process of dissolution can remove interspatial cements or mineral precipitates which will increase porosity and change the cementation factor in Eq. 1. Increasing porosity can decrease the membrane polarization effect (e.g., Slater et al. 2007). Changes in porosity will lead to variations in the bulk electrical conductivity which can be measured by the dc resistivity, induced polarization, and GPR methods.

Changes in surface area and surface roughness occur primarily from microbial mediated processes such as attachment to mineral surfaces. Bacteria have large surface area; hence, their attachment to mineral surfaces (e.g., Fig. 7b) enhances both the surface area and surface roughness. Increases in the surface roughness have been shown to enhance the imaginary conductivity component of complex conductivity (e.g., Abdel Aal et al. 2009). Increases in surface area can also result from decreases in grain size due to breakdown of minerals by organic acids (middle part of Fig. 6) and from the precipitation of nano-size particles (right side of Fig. 6) of different mineral phases either directly by the bacteria (e.g., magnetotactic bacteria directly precipitate magnetosomes) or by geochemical reactions mediated by the bacteria (Williams et al. 2005). Such changes can result in variability of pore-surface conductivity and pore-surface polarizability measurable by both dc and complex resistivity techniques (e.g., Davis et al. 2006; Ntarlagiannis et al. 2005a).

Changes in pore fluid chemistry (middle part of Fig. 6) can occur in a variety of ways including the direct addition of ions into solution from the production of organic acids, carbonic acids, and biosurfactants (biosurfactants can also change the wettability of the hydrocarbon contaminated sediments from oil wet to water wet (e.g., Cassidy et al. 2001)). Furthermore, enhanced weathering of minerals by organic and carbonic acids can release ions into solution. Microbial utilization of TEAs (e.g., NO_3^-, SO_4^{2-}) and the production of redox species (e.g., Fe^{2+}, Mn^{2+}) can also affect the solute concentration. Changes in pore

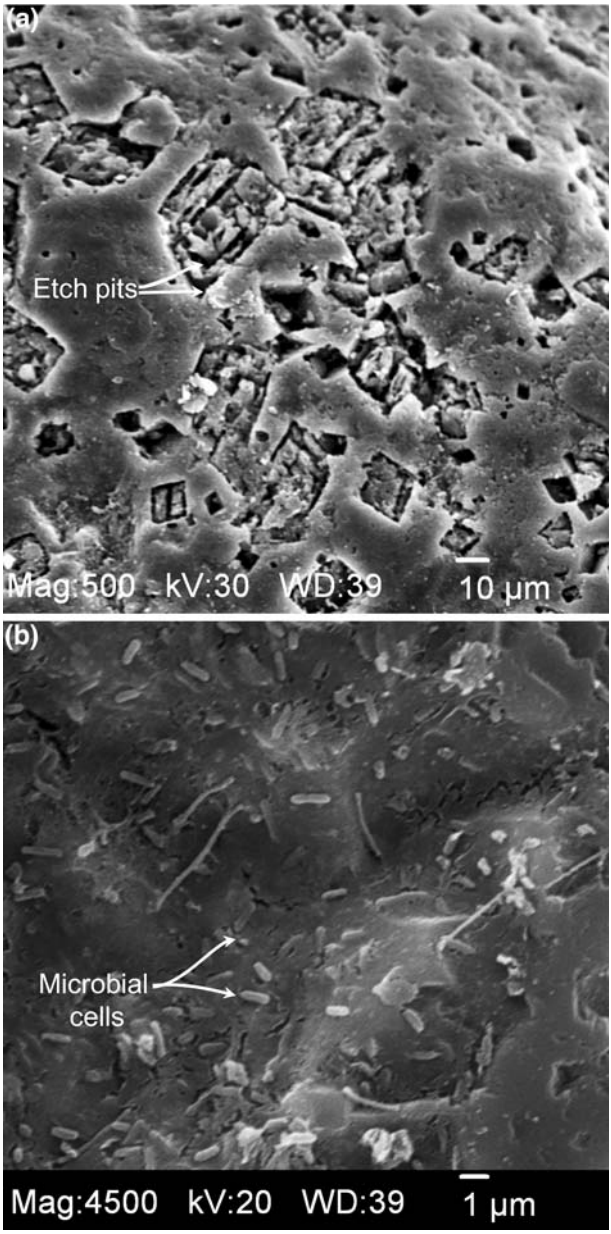

Fig. 7 Scanning electron microscopy image of sand from a light non-aqueous phase liquid (LNAPL) contaminated site showing **a** microbial related dissolution features such as etch pits and **b** bacteria/biofilm attached to sand surfaces

fluid chemistry directly result in changes in electrolytic conduction (Eq. 1) measurable by dc resistivity and complex conductivity (from variations in both the ionic charge density and ionic mobility), electromagnetic induction, GPR (increasing attenuation; Eq. 12), and SP (diffusion potentials; Eq. 14) techniques. Microbial driven redox reactions can cause

strong redox gradients (right side of Fig. 6) that generate a geobattery effect (e.g., Naudet et al. 2003; Naudet and Revil 2005) which is enhanced in the presence of conductive biofilms. Naudet et al. (2003) have shown a direct relationship between redox potential and SP anomalies and suggests that SP might be used as a proxy of redox potential at contaminated sites.

There are microbial processes and products at LNAPL-contaminated sites that in principle cause potential changes in the physical properties in the contaminated environment which are not used in routine geophysical investigations. These include, but are not limited to biogenic gases, precipitation of magnetic minerals, and temperature effects. The production of biogenic gases (e.g., CO_2, H_2S, H_2, and CH_4) can cause changes in the rheological properties of the contaminated region. Production of gases affect bulk electrical conductivity (middle part of Fig. 6), and can, cause an increase in GPR velocity as the gasses replace water with higher dielectric permittivity (Eq. 11). Biogenic gases can also result in the attenuation of acoustic wave amplitude. Williams et al. (2005) document a reduction in acoustic wave amplitude in a microbial induced mineral precipitation experiment. Davis (2009) has also documented a reduction in acoustic wave amplitude of up to 80% during microbial growth and biofilm formation in porous media. The Williams et al. (2005) and Davis (2009) studies suggest that the seismic method can be used to investigate the effects of microbial processes during bioremediation at LNAPL contaminated sites. However, there are no published works that document changes in acoustic wave amplitudes due to microbial processes at LNAPL contaminated sites. Petrophysical properties can be changed by the precipitation of magnetic mineral phases (e.g., magnetite) or magnetosomes from magnetotactic bacteria. Alteration of the magnetic properties of the contaminated media make magnetic methods useful as a survey technique at LNAPL contaminated sites. Microbial growth and chemical reactions in the contaminated region can cause increases in temperature. Such bio-induced temperature increases can potentially elevate the bulk electrical conductivity of the contaminated media. Atekwana et al. (2005) documented temperatures of 1–6°C higher within a hydrocarbon contaminated zone with anomalously higher bulk electrical conductivity compared to uncontaminated locations. Che-Alota et al. (2009) show that high temperatures associated with microbial activity in a LNAPL contaminated region decreased dramatically following remediation by soil vapor extraction.

Although dc resistivity, EM, and GPR techniques have been the techniques of choice to investigate LNAPL contaminated sites, the preceding discussion suggests that a variety of geophysical techniques can also be used to investigate microbial processes at these sites. Nonetheless, the biological and chemical changes in the contaminated environment are often coupled and are highly dynamic in time and space (e.g., Che-Alota et al. 2009). Different microbial community structures and processes occur at discrete depths in the contaminated subsurface due to patterned ecological successions, as the biological, physical, and chemical environments change spatially and temporally. Therefore, the interpretation of the geophysical data from LNAPL sites must be accompanied by an understanding of the fine-scale variations in microbial processes. We use Fig. 8 from Atekwana et al. (2005) to illustrate how microbial activity within narrow zones at discrete depth intervals at a LNAPL-contaminated site manifests in pore fluid chemistry and in the geophysical response. The geochemical data was acquired from closely spaced vertical intervals and the bulk electrical conductivity was measured from vertical resistivity probes. The results show that intervals with peaks in bulk electrical conductivity (Fig. 8a) were coincident with intervals with peaks in the total petroleum hydrocarbons (Fig. 8b), in the concentrations of major cations (e.g., Ca^{2+}; Fig. 8c), and TDS (Fig. 8d). These intervals

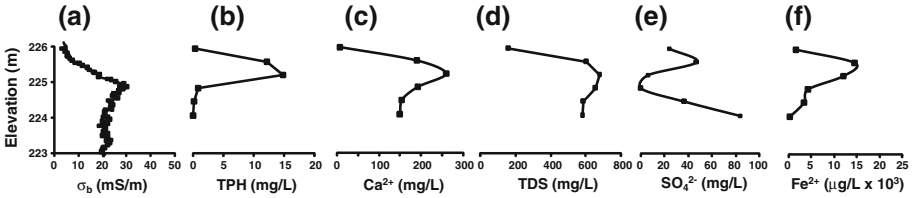

Fig. 8 Vertical profiles of (*a*) bulk electrical conductivity (σ_b), (*b*) total petroleum hydrocarbons (TPH), (*c*) Ca^{2+}, (*d*) TDS, (*e*) SO_4^{2-}, and (*f*) Fe^{2+} obtained from the saturated zone in an aquifer contaminated by light non-aqueous phase liquid (LNAPL). The chemical profiles show close correspondence with the vertical profile of bulk electrical conductivity (modified from Atekwana et al. 2005)

were zones of intense microbial activity as inferred from the utilization of TEAs (e.g., SO_4^{2-}; Fig. 8e) and the production of redox species (e.g., Fe^{2+}; Fig. 8f).

5 Biogeophysical Attributes of LNAPL Sites

Microbial activity varies spatially due to variability in the LNAPL (i.e., concentration and distribution) and will affect the physical property contrast between the uncontaminated background and the contaminated region. We illustrate this concept using Fig. 9 which shows a schematic of a hypothetical bulk electrical conductivity profile at a LNAPL contaminated site. We show the longitudinal (Fig. 9a), vertical (Fig. 9b), and transverse (Fig. 9c) bulk electrical conductivity profiles based on the LNAPL contamination depicted in Fig. 2. In the longitudinal profile, the maximum bulk electrical conductivity increase is associated with the source area which then decreases in the downgradient direction (Fig. 9a). The maximum increase in the bulk electrical conductivity in a vertical profile occurs within the source area within the smear zone where peak increases straddle the water table (Fig. 9b). Further downgradient beyond the source area, higher bulk electrical conductivity are observed within the plume (Fig. 9b). In transverse section, the bulk electrical conductivity is much higher for the contaminated region near the source zone (profile B–B′, Fig. 9c) compared to a more subtle increase downgradient from the source area (profile C–C′, Fig. 9c). Although we illustrate the biogeophysical attributes of LNAPL contamination undergoing bioremediation using the bulk electrical conductivity, similar conceptual models can be developed for all the other geophysical techniques. We now use field and laboratory studies to show how the ER, GPR, SP, and EM methods are used to characterize different biogeophysical attributes due to microbial processes.

5.1 Application of Surface Geophysical Techniques

We discuss a field example from the fire training site (FT-02) located at the decommissioned Wurtsmith Air Force Base in Oscoda, Michigan, USA (Sauck et al. 1998). This site has been investigated extensively over the last decade and has geochemical and biological data that can be used to aid geophysical interpretation. The subsurface at this site consists of clean, well sorted fine- to medium-grained sands which grade downward to gravel. Underlying the sand and gravel deposits at approximately 20 m is a silty clay unit 6.1–30.5 m thick. The average depth to the water table at the site ranges from 3.7 to 5.3 m. From 1958 to 1991, the US Air Force used the FT-02 site for bi-weekly fire training activities where several thousand liters of jet fuel and other hydrocarbons were combusted.

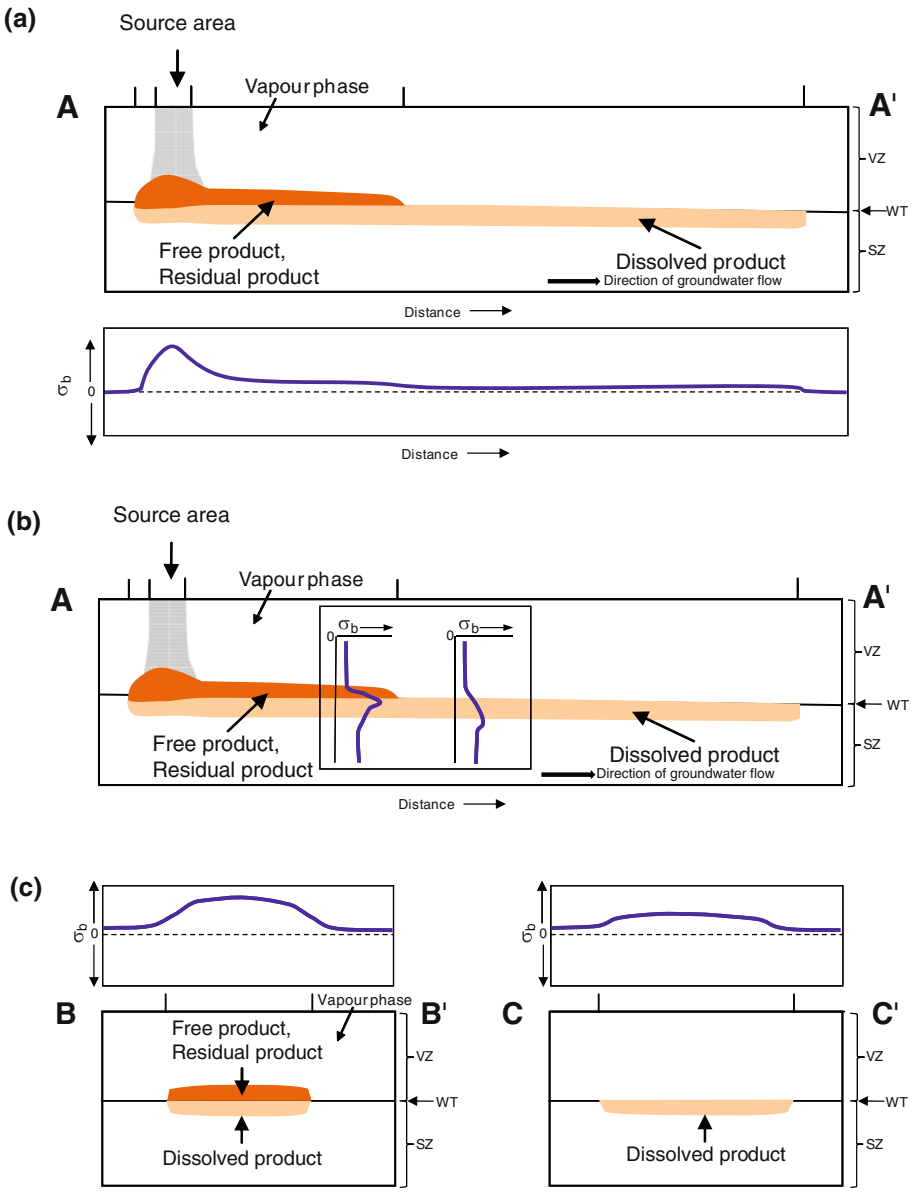

Fig. 9 Schematic of **a** the longitudinal, **b** vertical, and **c** transverse cross-sectional profiles of a hypothetical light non-aqueous phase liquid (LNAPL) spill showing corresponding variations in bulk electrical conductivity. The locations of the profiles are shown in Fig. 2a. The distribution of the vapour, residual, free, and dissolved phase LNAPL is shown in each panel. The bulk electrical conductivity response in the contaminated region is due to biodegradation. *VZ* is the vadose zone, *WT* is the water table, and *SZ* is the saturated zone. The direction of groundwater flow is shown by *arrows* in (**a**) and (**b**). Groundwater flow is *perpendicular* to the page in (**c**)

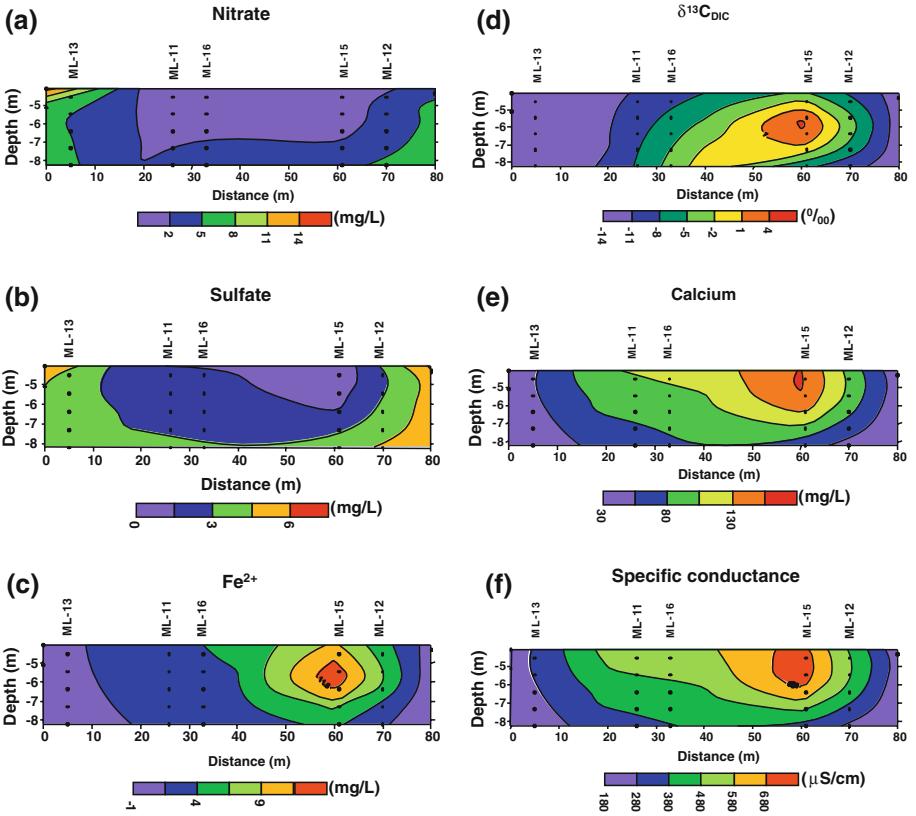

Fig. 10 Contoured vertical profiles of **a** nitrate, **b** sulfate, **c** Fe^{2+}, **d** isotope ratio of dissolved inorganic carbon ($\delta^{13}C_{DIC}$), **e** calcium, and **f** specific conductance from multi-level piezometers from the FT-02 light non-aqueous phase liquid (LNAPL) plume at the Wurtsmith Air Force Base in Oscoda, Michigan, USA. The multi-level piezometers are located downgradient from the source zone (Atekwana, unpublished)

Uncombusted hydrocarbons and combustion products seeped directly into the ground creating a LNAPL plume approximately 75 m wide and extending about 450 m downgradient from the source (Skubal et al. 2001). In the source area, both the vadose zone and saturated zones are impacted and free phase LNAPL occurs on top of the water table, whilst downgradient the contamination is in the dissolved phase (McGuire et al. 2000; Skubal et al. 2001).

Geochemical and microbial investigations of LNAPL contamination at this site indicate that biodegradation is occurring, and that methanogenesis is the dominant terminal electron process within the core of the plume (Chapelle et al. 1996; McGuire et al. 2000; Skubal et al. 2001). Figure 10 shows groundwater geochemical data collected from multi-level piezometers across the plume in the source area. The depletion of terminal electron acceptors such as nitrate (Fig. 10a) and sulfate (Fig. 10b) and the high concentrations of Fe^{2+} (Fig. 10c) a redox species is evidence of biodegradation of LNAPL in the plume. TEAs processes have advanced to the methanogenesis stage which is inferred from very positive (>0‰) values in the stable carbon isotope ratio of dissolved inorganic carbon ($\delta^{13}C_{DIC}$) in the plume core (Fig. 10d). Major ion chemistry suggests that enhanced mineral weathering is occurring within the contaminated aquifer with elevated values of

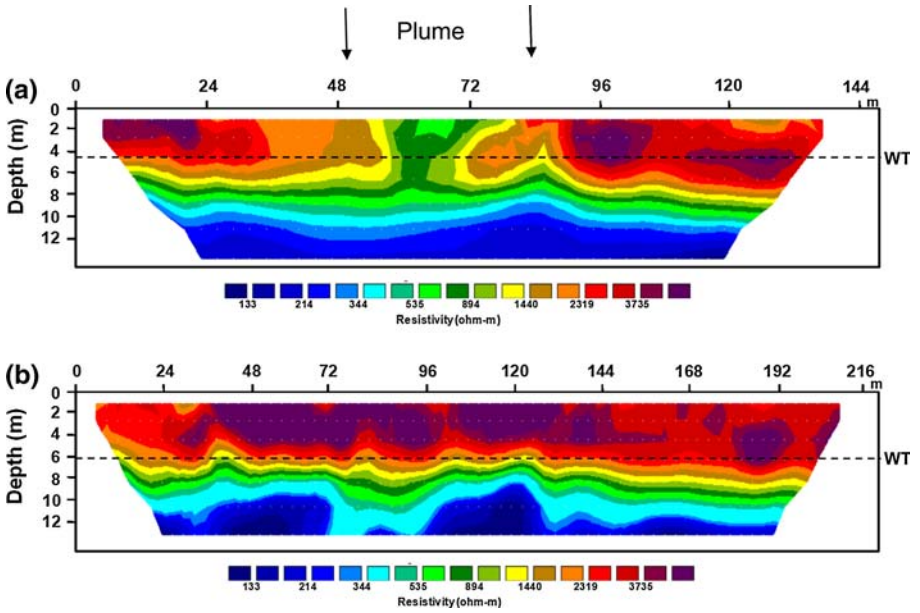

Fig. 11 Bulk electrical resistivity profile near the source zone at a light non-aqueous phase liquid (LNAPL) contaminated site (FT-02) at the Wurtsmith Air Force Base, Oscoda, Michigan USA showing **a** profile from an area near the source zone shown in the profile B–B′ in Fig. 2a and **b** profile across a distal portion of the plume represented by profile C–C′ in Fig. 2a. WT is the water table

Ca^{2+} (Fig. 10e) and groundwater specific conductance (Fig. 10f). The zone of active biodegradation is limited to the upper parts of the saturated zone contaminated by dissolved LNAPL and is ∼2–3 m thick (Che-Alota et al. 2009).

Figure 11a shows an electrical resistivity profile obtained across the source zone. This profile is similar in location to the hypothetical cross section B–B′ in Fig. 2a that is depicted in profile B–B′ in Fig. 9c. The survey consisted of a dipole–dipole resistivity array at 3 m electrode spacing using a 10-channel IRIS Syscal Pro resistivity system with 72 electrodes. The profile clearly shows a low resistivity anomaly at horizontal location 48–85 m. The low resistivity anomaly is mostly prominent in the vadose zone, but extends from the surface into the saturated zone. The contribution of biodegradation in the vadose zone to the geophysical signature is in stark contrast to downgradient locations where the contamination exists only in the dissolved phase. Figure 11b is a resistivity profile obtained from a downgradient location at the FT-02 plume. An equivalent location is shown in cross section C–C′ in Fig. 2c and depicted in profile C–C′ in Fig. 9c. The profile from this downgradient location does not show anomalously low electrical resistivity across the plume, despite the fact that active biodegradation is occurring in the plume at this location indicated by relatively high TDS and metals and low TEAs. The above resistivity profiles illustrate the fact that varied responses can be obtained from different locations at the same site using the same geophysical technique.

A GPR profile (Fig. 12a) was acquired near the source zone across the FT-02 plume by Bradford (2007). The data were acquired with 100-MHz antennas in continuous CMP mode with a 25-fold common–source gathers, 0.6-m source interval, and a 0.3-m receiver interval. See Bradford (2007) for details on data processing and computation of the dispersion parameter (D) shown in Fig. 12b. The dispersion parameter is useful for identifying

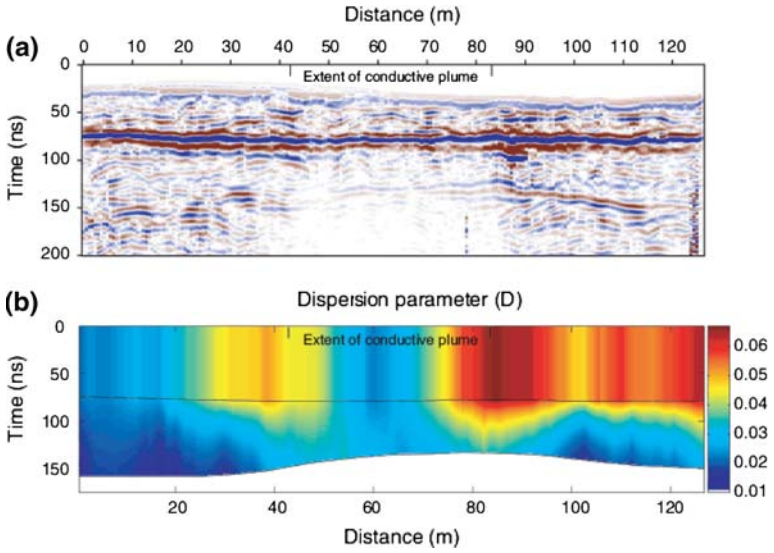

Fig. 12 **a** Ground penetrating radar (GPR) acquired near the source zone at a light non-aqueous phase liquid (LNAPL) contaminated site (FT-02) at the Wurtsmith Air Force Base, Oscoda, Michigan, USA, showing **a** CMP 25-fold stack of 100-MHz data and **b** image of the distribution of the dispersion parameter (D) calculated from the GPR spectral data. The zone of increased dispersion corresponds to the region of increased DC conductivity at the site (e.g., Fig. 10). The water table reflector is located at about 65 ns (modified from Bradford 2007)

subsurface anomalies from GPR spectral data and is large for geologic media with strong dispersion and small for weak dispersive media. The GPR profile (Fig. 12a) shows a zone of attenuated signals beginning immediately below the water table and extending to deeper depths and is similar to the results of other GPR profiles near the source area (Sauck et al. 1998; Che-Alota et al. 2009). The dispersion distribution (Fig. 12b) shows a distinct zone of strong dispersion coincident with the zone of GPR signal attenuation, with the dispersion generally stronger in the vadose zone than in the saturated zone. The spatial position of the dispersion zone in the Bradford (2007) study corresponds to the region of anomalously low resistivity observed in the vadose zone (Fig. 11a). Bradford (2007) suggests that increased DC conductivity of the aquifer pore fluids alter the relaxation characteristics of the bulk formation, masking decreases in dispersion caused by the residual LNAPL in the vadose zone. The resistivity (Fig. 11a) and GPR (Fig. 12a) results collected near the source area with LNAPL impact in the vadose zone suggest significant enhancement of the geophysical signal from higher pore water conductivity due to biodegradation in the vadose zone.

Although the surface electrical resistivity survey was unable to image the plume at the downgradient location (Fig. 11b), GPR investigations at the same downgradient locations clearly delineate the plume. In fact, GPR surveys near the source zone and downgradient locations are characterized by GPR shadow zones, which were used to map the transverse extent of the contaminated region along a longitudinal profile (see Sauck et al. 1998 for additional details). It appears that the higher resolution of the GPR technique is more suitable for imaging smaller vertical increases in bulk formation conductivity than the resistivity technique when deployed from the surface.

An SP survey over the FT-02 contaminated study site in 1996 (Fig. 13a) shows a positive (10–25 mV) SP anomaly over the lateral extent of the contamination (Sauck et al.

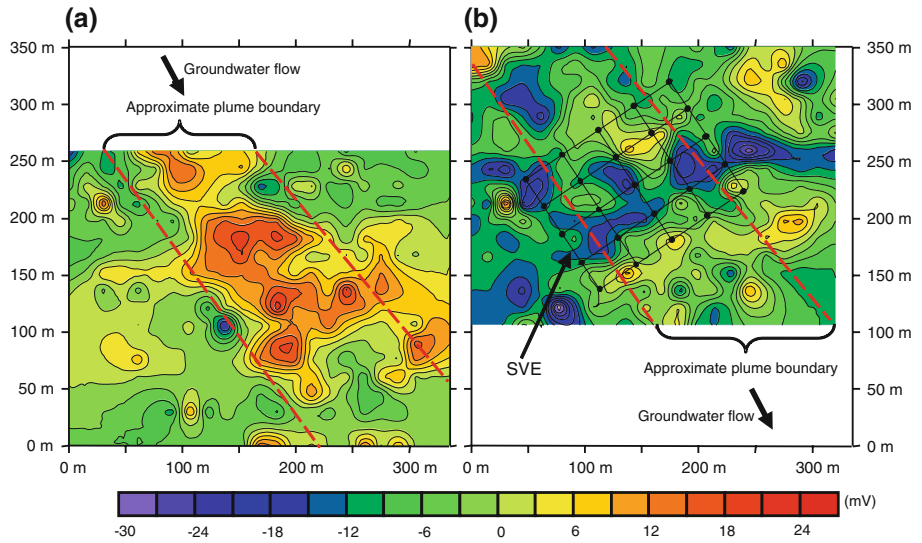

Fig. 13 Self potential (SP) anomaly map near the source area at a light non-aqueous phase liquid (LNAPL) contaminated site (FT-02) at the Wurtsmith Air Force Base, Oscoda, Michigan, USA measured in **a** 1996 and **b** 2007. The positive anomaly observed in 1996 is no longer seen in 2007 due to remediation of the area by the vapor extraction technique. A grid showing the soil vapor extraction (SVE) system is superimposed on the 2007 SP grid (adapted from Che-Alota et al. 2009)

1998). Sauck et al. (1998) relate the source mechanism of the SP anomaly to diffusion (or membrane) potentials (Eq. 14) associated with chemical concentration gradients due to the mobility of ionic charge carriers. The chemical gradients are the result of microbial mediated redox processes occurring in the contaminated aquifer during intrinsic bioremediation (e.g., see Fig. 10). Remediation of the source area at this site was initiated in 2001, and consisted of soil vapor extraction from the source zone at 25 extraction points in a grid-like fashion (Fig. 13b). SP surveys in 2007 showed that the positive SP anomaly had disappeared from the contaminated region (Fig. 13b), although geochemical surveys in 2007 still showed an active dissolved phase plume in the survey location (Atekwana, unpublished). Therefore, the disappearance of the positive SP anomaly clearly demonstrates the effects of microbial processes in the vadose zone on the generation of the SP signals.

5.2 Application of Downhole Geophysical Surveys

The vertical variability of microbial processes at LNAPL contaminated sites is due in part to the partitioning of LNAPL into different phases, the vertical distribution of TEAs, and variations in the micro-environment. The variations in the geophysical signatures that can be expected at LNAPL contaminated sites are schematically depicted by Fig. 9b. We use a field example from an old oil refinery in Carson City, Michigan, USA to demonstrate the effectiveness of vertical geophysical profiling of microbial alteration of LNAPL at contaminated sites (Atekwana et al. 2000; 2004a, b, c; Werkema et al. 2003). Over a 50 year period, continuous hydrocarbon releases (mostly JP4 jet fuel and diesel) from storage facilities and pipelines resulted in the seepage of petroleum hydrocarbons into the subsurface which contaminated soil and groundwater. The contaminated zone is approximately 4.6–6.1 m

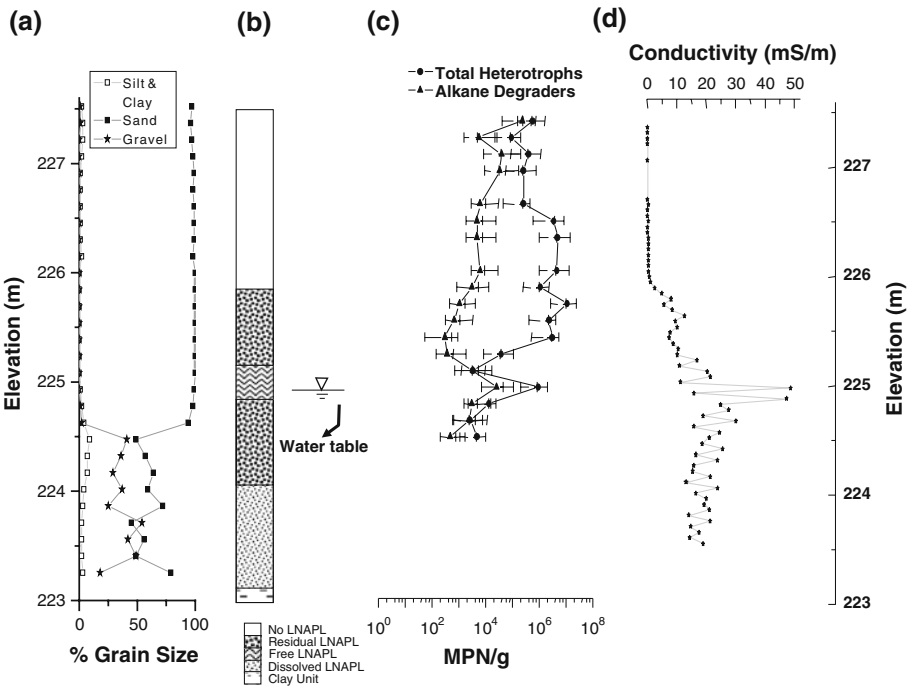

Fig. 14 Depth distribution of **a** grain size, **b** light non-aqueous phase liquid (LNAPL) phases, **c** microbial population numbers, and **d** bulk electrical conductivity obtained from a LNAPL contaminated site at the Crystal Refinery in Carson City, Michigan, USA (adapted from Atekwana et al. 2004a)

thick. The vadose zone is characterized by fine- to medium-grained sands, while the saturated zone consists of medium-sized sands and gravels underlain by a clay unit (Fig. 14a).

The distribution of the different phases of LNAPL contamination is shown in Fig. 14b. A 30 cm free phase LNAPL floating on the water table is located between a residual phase LNAPL that is 75 cm above the free phase and a dissolved LNAPL that extends about 75 cm below the water table. The water table occurs at an elevation of 224.75 m. The smear zone consists of the top of the region contaminated by residual LNAPL to about 25 cm below the water table. The vertical distribution of aerobic heterotrophic and oil degrading microbial populations is shown in Fig. 14c, and depicts higher oil degrading microbial populations in the residual and free phase zones mainly above the water table (see Atekwana et al. 2004b for more details). The bulk electrical conductivity was measured using a 5.0 cm Wenner array from in situ vertical resistivity probes (VRPs) installed from the surface to the top of the clay unit (Fig. 14d). Anomalously high bulk electrical conductivity is coincident with the smear zone impacted by residual and free LNAPL and concomitant with a higher percentage of oil degrading microbial populations (Fig. 14c, d).

SEM images (Fig. 15a) from the zone of anomalously high bulk electrical conductivity show that mineral grain surfaces are highly etched and pitted, compared to images from the uncontaminated zones (not shown). The SEM images from within the contaminated regions also show extensive development of bacterial biofilms (Fig. 15b). Furthermore, molecular analyses determined by construction and evaluation of 16S rRNA gene libraries show spatial heterogeneity in the microbial community structure that parallel the vertical changes in bulk electrical conductivity (Allen et al. 2007). Diversity indices analyses

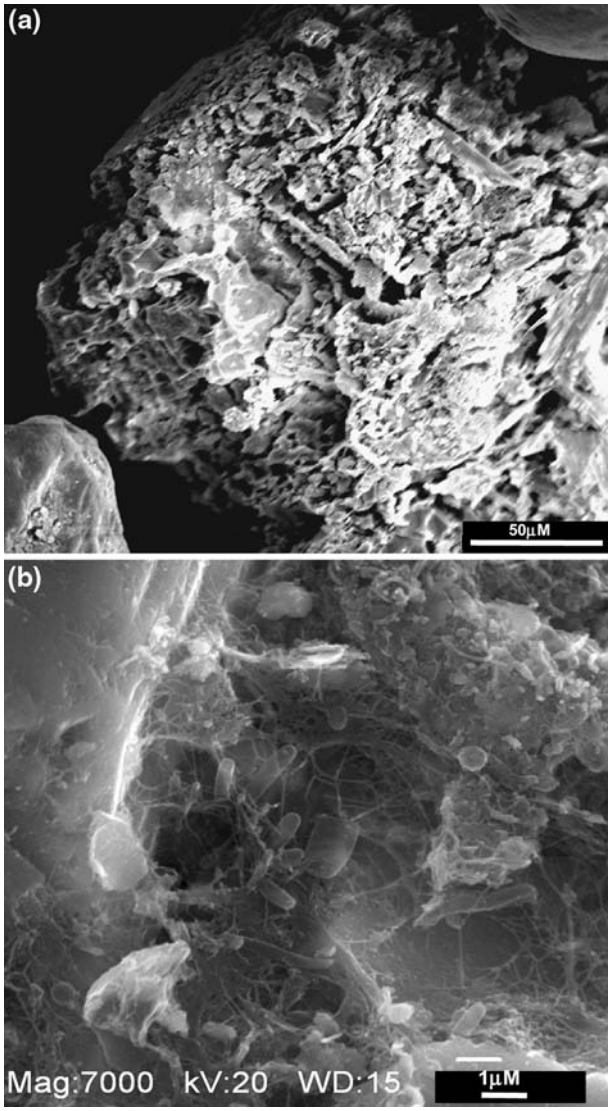

Fig. 15 Scanning electron microscopy image of **a** weathered mineral surface and **b** microbial biofilm attached to a mineral surface obtained from a light non-aqueous phase liquid (LNAPL) contaminated site at the Crystal Refinery in Carson City, Michigan USA (adapted from Atekwana et al. 2004a)

revealed that, at the contaminated locations, there was less diversity within the microbial community (Allen et al. 2007). More importantly, a multivariate statistical analysis of the relationship between the bulk electrical conductivity, the lithology, and the microbial communities indicated a direct correlation between specific microbial populations (e.g., syntrophic species *δ- and ε-Proteobacteria)* and higher bulk electrical conductivity. These results are the first to suggest that the elevated bulk electrical conductivity observed at LNAPL contaminated sites may be related to the presence and activities of specific microbial populations. The Allen et al. (2007) study demonstrates the potential for using variations in the bulk electrical conductivity (and other geophysical properties) to guide soil and sediment sampling from discrete depths within the contaminated subsurface for microbial ecology studies.

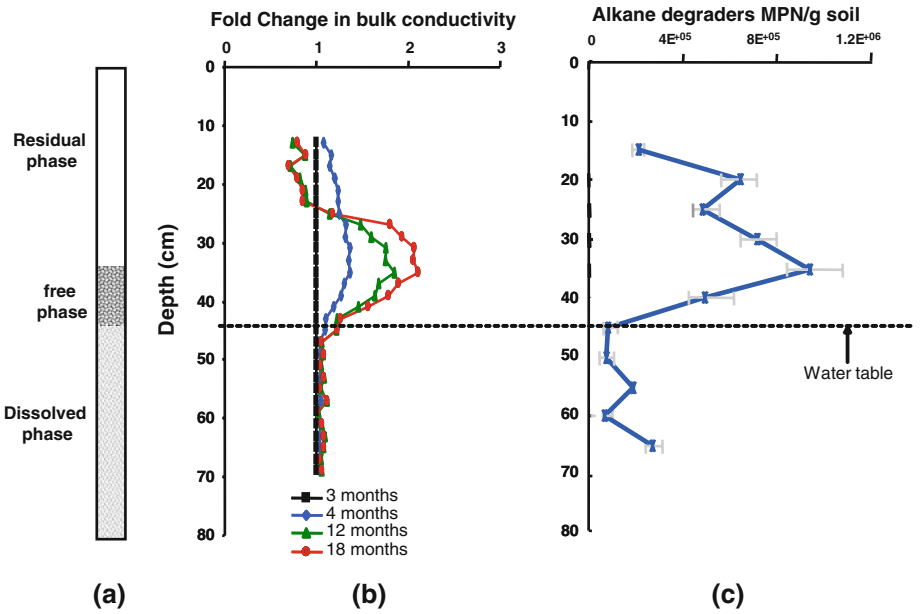

Fig. 16 Depth distribution of **a** light non-aqueous phase liquid (LNAPL) phases, **b** bulk electrical conductivity, and **c** oil degrading microbial (alkane degraders) populations from a laboratory meso-scale biodegradation experiment. The microbial populations were obtained after 20 months into the experiment

The results from the Carson City site were replicated in a laboratory column experiment conducted over 24-month period by Atekwana et al. (2004d). The aim of this experiment was to investigate the effects of biodegradtion on bulk electrical conductivity. The columns consist of biotic contaminated and uncontaminated columns which were 80 cm long and constructed of 31 cm diameter polyvinyl chloride pipe (PVC) pipe. The columns were filled with autoclaved fine- to medium-grained sands collected from a field site in Carson City Michigan, USA. The uncontaminated column contained water and nutrients, while the contaminated column was amended with 4 L of diesel. Diesel sorbed on the sand (residual phase) occurred from 0 to 32 cm, sands contaminated with free phase diesel occurred from 32 to 45 cm, and dissolved phase diesel contamination occurred in the water saturated zone below 45 cm (Fig. 16a). The columns were maintained at room temperature (23–25°C) for the duration of the experiment. The results showed that the largest increase in the bulk electrical conductivity (>120%) occured in the capillary fringe and smear zone compared to a 10% change in the saturated zone (Fig. 16b). Microbial enumeration showed that the highest population of oil degrading microorganisms did not occur below the water table where the hydrocarbons were mostly in the dissolved phase, but were directly correlated with the zone of higher bulk electrial conductivity in the smear zone (Fig. 16c). In the field setting, it is likely that the fluctuating water table smears the LNAPL, potentially making it more readily available for microbial activity (Lee et al. 2001). The high concentrations of total petroleum hydrocarbons and the availability of TEAs and nutrients brought in by seasonal recharge events stimulate microbial activity and make this a zone of the most active/intense biodegradation, hence the zone of the highest alteration.

The above findings by Atekwana et al. (2004d) are consistent with recent studies by Cassidy (2007, 2008) that document maximum GPR attenuation within the smear zone at a LNAPL contaminated site. From GPR signal attribute analysis and a dielectric property comparison between LNAPL contaminated and uncontaminated areas, Cassidy (2007) documented that the most significant and identifiable zone of attenuation was the smear zone, where the attenuation could be wholly related to material property loses (>2–6 dB/m). The smear zone also had a slight but observable frequency dependence to the attenuation spectrum with the lowest frequency data (<300 MHz) showing the greatest degree of loss. Measurements from pure LNAPL and the vadose zone showed little signal attenuation. Cassidy (2007) also noted that attenuation attributes from the saturated zone at the contaminated location were not significantly different from attenuation characteristics from the saturated zone in an uncontaminated area. Hence, the results of the Cassidy (2007) study are consistent with observations of anomalously high bulk electrical conductivity of aged LNAPL contamination at the Carson City refinery site (Atekwana et al. 2004a).

5.3 The Effect of Microbial Activity on the Interfacial Electrical Properties

SEM images from LNAPL contaminated sites undergoing remediation (Figs. 7a, b; 15a, b) show marked changes in the grain surface characteristics. It is expected that the volume of the aquifer material altered in this manner will exhibit distinct interfacial electrical properties related to the direct and indirect alteration of aquifer minerals by microbial activities. Studies conducted by Abdel Aal et al. (2006) clearly demonstrate that microbial processes induce changes in the interfacial properties of sediments and impact the geophysical response. Abdel Aal et al. (2006) obtained complex conductivity measurements from sediment cores retrieved from the Carson City site discussed in Sect. 5.2 (See Abdel Aal et al. (2006) for details on complex conductivity measurements). The highest imaginary conductivity and phase values were observed for samples from the smear zone (where contamination was mostly in the residual and free phases), which exceeded the values obtained for samples contaminated with dissolved phase LNAPL. The samples contaminated by dissolved phase LNAPL had imaginary conductivity values that exceeded values obtained for uncontaminated samples. Real conductivity values, although generally elevated for samples from the smear zone, did not show a strong correlation with contamination. These results suggest that there are distinct differences in the magnitude of the polarization of the samples from locations contaminated with different LNAPL phases. Because the imaginary conductivity is largely dependent on surface area, Abdel Aal et al. (2006) suggest that the accumulation of microbial cells with high surface areas at the mineral-electrolyte interface are largely responsible for the imaginary conductivity response. Bacterial cell surfaces are charged, highly complex, and are analogous to colloidal particles (Poortinga et al. 2002). Therefore, polarization of the ions in the electrical double layer at the bacterial-mineral-fluid interface depends on the mobility of the counterions in the Stern layer, surface charge density, and the surface area of the grains (Abdel Aal et al. 2009). Microbial attachment to mineral surfaces increases the surface roughness causing an increase in the polarization magnitude. The large surface area of the bacteria accentuates this effect. The SEM images which show a very rough and highly weathered mineral grain (Fig. 15a) and which show significant attachment of bacteria and biofilms on a mineral surface (Fig. 15b) obtained from a region contaminated by LNAPL at the Carson City site support this hypothesis.

5.4 The Effect of Microbial Activity on Electromagnetic Response

Atekwana et al. (2002) used the electromagnetic method to investigate part of a former petroleum refinery site in Kalamazoo, Michigan, USA. Leakage from storage tanks resulted in the contamination of the subsurface sediments and groundwater by refined hydrocarbons and hydrocarbon sludge dumped at the site. Although most of the remediation activities at the site focused on free phase hydrocarbon removal, significant contamination of the vadose zone remained. The sediments at the site are characterized by glacial till, outwash sand, and gravel. The water table in the study area is approximately 6–8 m below the surface.

An EM survey using the Geonics EM-31 MK2 was conducted at the site to map the extent of shallow subsurface contamination. The data from the out-of-phase component presented in Fig. 17 show a broad zone of high conductivity values in the West to North West part of the survey area extending from an anomalies due to the presence of a pipe. Background conductivity values at the site are <13 mS/m but are between 15 and 20 mS/m within the contaminated zone. The sources of the conductivity anomaly are inferred to occur within the vadose zone, because the top of the zone of saturation is considerably deeper (>6 m) than the depth limit of detection of the EM-31 instrument. This instrument,

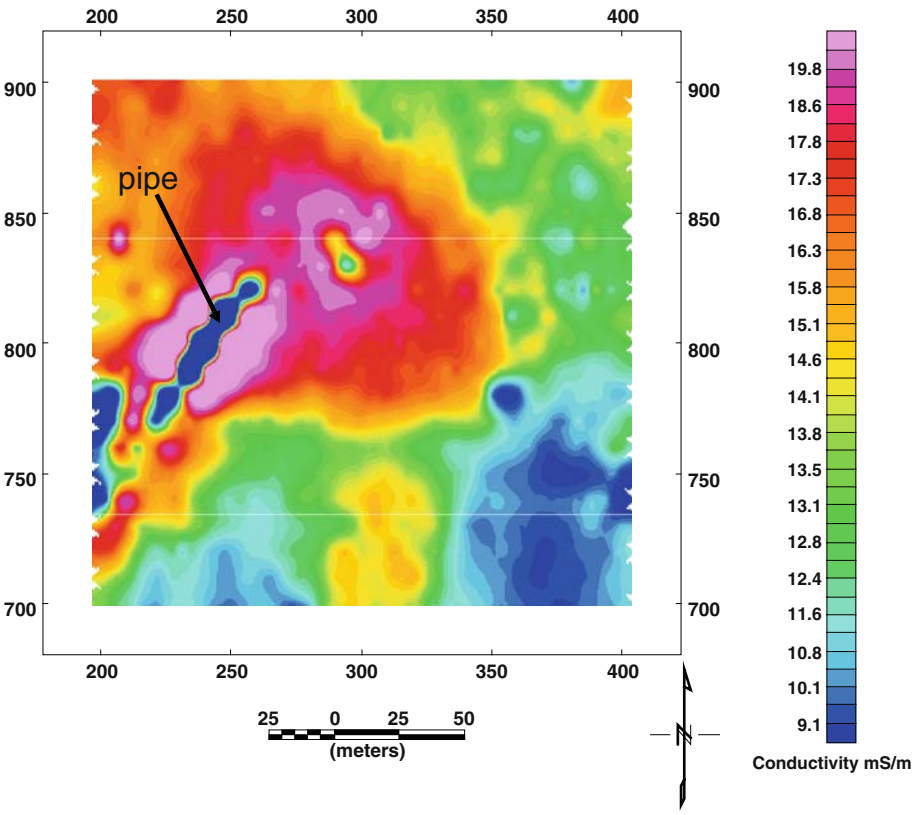

Fig. 17 EM 31 conductivity distribution at a light non-aqueous phase liquid (LNAPL) contaminated site in Kalamazoo, Michigan, USA. The anomalous high conductivity is due to biodegradation of LNAPL perched in the vadose zone (adapted from Atekwana et al. 2002)

with 3.66 m coil separation, receives most of its response from the 1–3-m depth interval when deployed in the normal (horizontal coils) position. Soil borings from within the anomalous conductivity zones confirmed the presence of perched hydrocarbon zones associated with the high conductivities. Atekwana et al. (2002) suggest that the high conductivities result from an increase in pore fluid conductivity due to ions released during biodegradation of LNAPLs trapped in the vadose zone.

5.5 Non Conductive Geophysical Signatures Associated with Long-Term LNAPL Contaminated Sites

Not all "aged LNAPL plumes" exhibit anomalous geophysical signatures associated with biodegradation. Tezkan et al. (2005) investigated an "aged" hydrocarbon contaminated site at a refinery 60 km North of Bucharest in Romania. The first reports of hydrocarbon contamination occurred in 1974 when oil contamination was documented from domestic wells in nearby villages. The thickness of the free hydrocarbon at the time of the geophysical investigations varied, but was up to 4.8-m thick beneath the central part of the refinery. The subsurface geology was characterized by Quaternary river deposits and the aquifer consisted of a thin top soil horizon and a clay layer underlain by unconsolidated sands and fine to coarse gravels. Significant fluctuations in the water table level occurrs at the site due to recharge events, ranging from 5–8 m during dry periods to $\sim$1 m during wet periods. Hence, it is expected that a significant smear zone would have developed at this site.

Geophysical surveys at this site were conducted outside the perimeter of the refinery at a location where the hydrocarbon was $\sim$1 m thick. The RMT was used to investigate the contamination. By the time of the survey, the contamination could be considered "aged" as the geophysical surveys took place in 1999, approximately 25 years after the first occurrence of hydrocarbon contamination was reported. We would expect that if biodegradation was occurring at this site then a conductive signature would be observed. Instead, 2D-inversion results for several profiles (Fig. 18a) show a resistive layer below a conductive surface layer from 3 to 13 m. Existing boreholes indicate that the resistive structure was associated with hydrocarbon contamination. A comparison with background locations (Fig. 18b) suggests that the resistivity of the contaminated area was higher than that of the background location, especially at higher frequencies. Laboratory measurements of fluid samples taken from the contaminated zone showed a very high resistivity for the oil (10^7 Ωm), whereas the resistivity of the water was about 3 Ωm because of possible biodegradation. Tezkan et al. (2005) concluded that the overall contaminated zone was highly resistive despite a conductive plume beneath the resistive oil layer. It is possible that the thicker resistive zone masked the thinner conductive layer.

This observation of a high resistive layer associated with LNAPL contamination overlying a conductive groundwater plume (probably the result of biodegradation) has also been documented by Benson et al. (1997) and Frohlich et al. (2008). Although no comprehensive chemical and biological data was provided, the results suggest that high resistivity anomalies associated with the presence of LNAPLs can persist even after decades of contamination. Without the full geochemistry and biological data it is difficult to assess the state of biodegradation at these sites.

A study by Petterssen and Nobes (2003) also reported resistive signatures from electromagnetic induction surveys from hydrocarbon contamination at the Scott Base, Antarctica. A GPR survey at the same site was not successful in mapping the contaminated region. Although the age of contamination is unknown, the base was constructed in 1957 and occupied permanently in 1962 (Petterssen and Nobes 2003). It is possible that

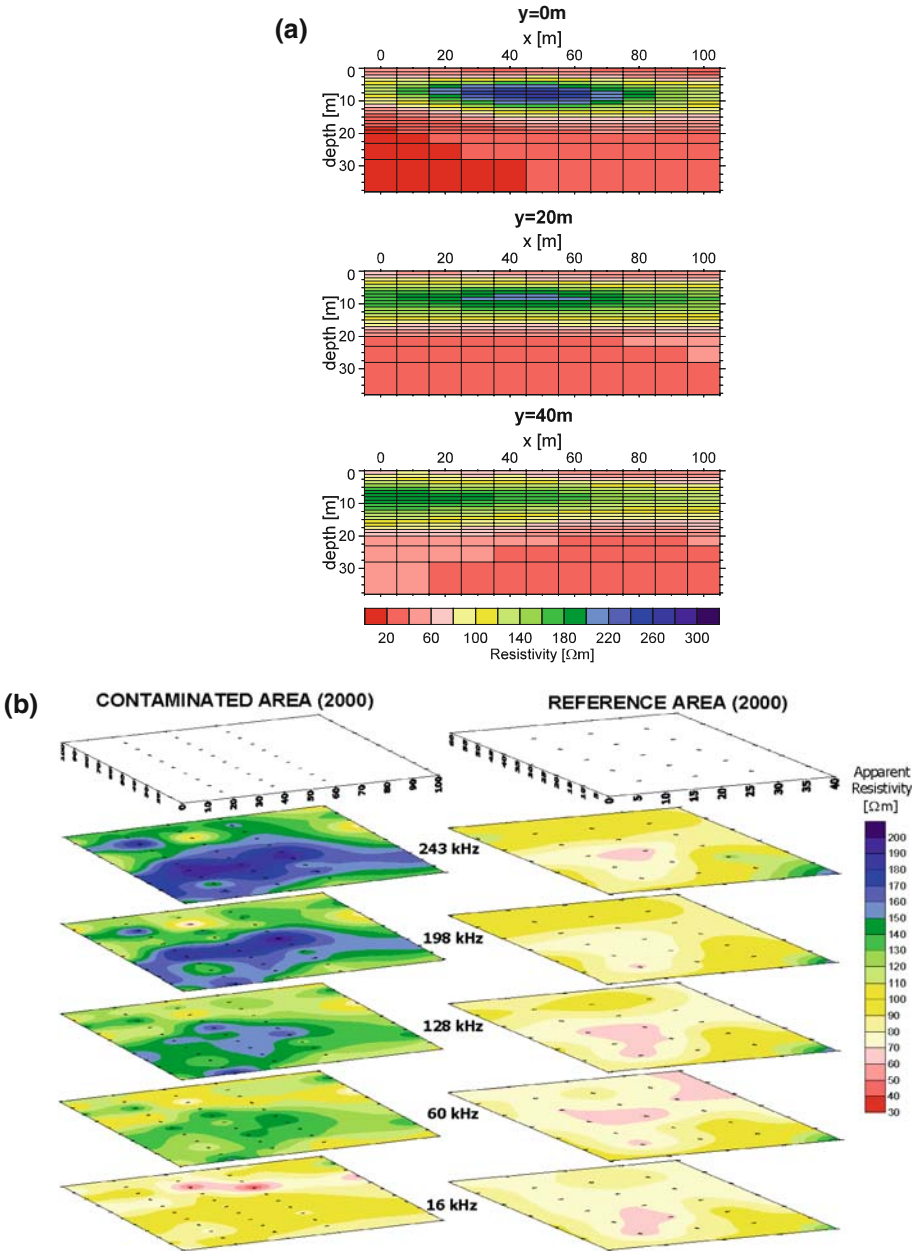

Fig. 18 **a** 2D resistivity distribution along several profiles (0, 20, and 40) at a light non-aqueous phase liquid (LNAPL) contaminated site in Bucharest, Romania and **b** comparison of the apparent resistivities of the contaminated location and the reference (background) location (adapted from Tezkan et al. 2005)

contamination at the site could be as old as 46 years before the geophysical surveys were conducted. Nevertheless, the resistive signature of the plume was still apparent. We speculate that the extreme cold weather conditions may inhibit the activity of the bacteria.

Biodegradation occurs only when microbial populations capable of degrading the hydrocarbons have favorable moisture and nutrient conditions (Haack and Bekins 2000). Without information on the microbial conditions at the site, it is difficult to assess the extent of LNAPL alteration and its impact on the geophysical signatures.

6 Summary and Conclusions

Microbial transformation of LNAPL in the contaminated subsurface results in a complex bio-physicochemical environment. The presence, types, and distribution of different microbial populations are dictated by the distribution and concentration of organic carbon from the LNAPL contamination that serves as the electron donor and on the terminal electron donor-electron acceptor processes that drive LNAPL biodegradation. A review of the pertinent literature relating microbial activity to changes in the geophysical properties at LNAPL contaminated sites suggests that microbial activity causes profound changes in the subsurface environment in three major ways as summarized in Fig. 6: (1) by the production of biomass and development of biofilms that alter the surface properties of aquifer minerals and cause changes in pore volume characteristics of the aquifer, (2) by the generation of metabolic byproducts that weather aquifer minerals altering the ionic concentrations of the aquifer pore fluids and changing the saturation states of minerals in the aquifer, and (3) by mediating geochemical reactions that cause changes in the redox state resulting in distinct redox zonations.

Direct attachment of microbes on mineral surfaces and the development of biofilms alter the surface electrical properties because of the electrical charge associated with microbes and the increase in surface area and roughness imparted onto minerals by the large surface area of microbes. In addition, growth of microbes in colonies and as biofilms in pores of the aquifer matrix change the pore volume characteristics (e.g., porosity). Geophysical techniques that are sensitive to changes in the interface properties between mineral, water, and microbes (e.g., complex conductivity) are capable of sensing this aspect of microbial alteration of the contaminated matrix.

During biodegradation, the pore fluid chemistry is changed by the degradation of the LNAPL (decrease in LNAPL concentration), decrease in the TEAs (e.g., NO_3^-, SO_4^{2-}), the production of redox species (e.g., Fe^{2+} and Mn^{2+}), and production of metabolic byproducts such as organic acids, biosurfactants, and biogenic gases (e.g., CO_2, H_2, CH_4, H_2S). The decrease in TEAs and the production of redox species will change the ionic concentration of the pore fluids and affect geophysical techniques sensitive to the electrical conductivity of the pore fluids (e.g., ER, IP, and GPR) and in the concentration in ionic gradient and redox species (e.g., SP). The byproducts of microbial action such as organic and carbonic acid (from dissolution of CO_2) will weather aquifer minerals. A combination of mineral dissolution by microbial action and their byproducts will produce solute species that will change the saturation state of minerals and result in dissolution or precipitation of various mineral phases. The precipitation of mineral phases from oversaturation will alter mineral surfaces and the pore structure of the aquifer detectable by geophysical techniques such as ER and IP. Other bio-induced transformations such as increased temperature can also affect a variety of geophysical properties (e.g., higher pore water temperatures can increase the bulk electrical conductivity).

The geophysical signature of the contaminated region depend on factors such as the type of the LNAPL (crude oil, jet fuel, diesel fuel), LNAPL release history (e.g., continuous release or single release), the distribution of the LNAPL relative to air in the vadose zone

or water in the saturated zone, hydrologic processes (e.g., advective transport, seasonal recharge), the saturation history of the contaminated media and biological processes. The degree to which LNAPL biodegradation occurs depend on the environmental conditions as determined by subsurface geology, temperature, moisture content, and microbial activity. Field and laboratory studies of the geophysical response of LNAPL contamination undergoing bioremediation is detectable by geophysical techniques for situations in which microbial processes create contrast in the physical properties in the altered contaminated region that is sufficiently different from the unaltered LNAPL and from background.

The biological and chemical changes responsible for the changes in the geophysical properties in the contaminated environment often occur at discrete depth intervals. Different microbial community structures and processes occur at fine scale (< cm scale) due to patterned ecological successions, as the biological, physical, and chemical environments change spatially and temporally. Therefore, the interpretation of the geophysical data from LNAPL sites must be accompanied by an understanding of the fine-scale variations in microbial processes. Hence, the successful application of any geophysical technique at LNAPL contaminated sites must be guided by a proper understanding of the factors that govern the geophysical response and which of the factors are likely to dominate the geophysical response. We find that maximum changes in geophysical signatures occur in the tension saturated, capillary, and upper portion of the saturation zones. It is within these zones that the highest populations of oil degrading microorganisms occur and the maximum changes in geophysical signatures (increased conductivity, maximum attenuation of GPR signal amplitudes etc.) are likely to be observed.

The subsurface region altered by microbial processes is akin to a target, whereby its detection by geophysical techniques is scale dependent. The distribution of the different LNAPL phases is spatially variable; thus, geophysical surveys in and near the source area with contamination in the vapor, residual, free, and dissolve phase will provide a response different from a similar survey downgradient of the source area contaminated only by dissolved phase. The volume (lateral and horizontal extent and vertical thickness) of contaminated aquifer to be imaged by geophysical techniques needs to be known and the expected changes in the physical properties are key to choosing a geophysical technique for investigation. The volume of aquifer (e.g., thickness) contaminated will also determine the survey design appropriate for resolving the target region. In addition, the choice of geophysical techniques to be employed is usually determined by instrument availability. Nevertheless, the resolution of the instrument for the type of survey to be conducted needs to be evaluated by the investigator. This review does not cover such matters because site characteristics will vary from place to place, requiring the survey design to be tailored to each site. Ideally, prior to conducting geophysical surveys, the following should be considered: (1) the distribution of the different phases of the LNAPL contamination, (2) the relative volume of the subsurface impacted by the different phases, (3) the nature and extent of LNAPL alteration (e.g., physical, chemical and biological), (4) the ratio of the mass of biologically altered LNAPL relative to the mass of the unaltered LNAPL, and (5) the effect of changes in the physical properties of the contaminated media imparted by physical, chemical and biological alteration of the LNAPL. In situations where a large volume of the LNAPL remains unaltered, evidence of microbial degradation of the altered mass, although present in the aquifer might go undetected in the geophysical results. In this case, high resolution downhole geophysical techniques might be able to resolve the zones of enhanced microbial activity.

Geophysical investigations can be effectively used to assess biogeochemical processes at field settings and in laboratory experiments. However, this is by no means a trivial task.

It is difficult to assess the extent of microbial induced alterations because microbial transformations of the contaminated environment are often coupled and dynamic, and occur over a wide range of spatial and temporal scales. For example, changes in pore fluid conductivity may result from both hydrologic processes (e.g., advective flow due due to seasonal recharge) and microbial processes (e.g., mineral precipitation), while changes in porosity resulting from the disolution of a particular mineral may occur concurrently with bio-induced mineral precipitation of another mineral species. Future research should focus on isolating the effects of these coupled processes and quantifying their contributions to geophysical property changes. Significant challenges remain to be overcome such as issues of scaling of the geophyscal signals of bulk property changes to the microbial processes from the micro- to the nano-scale of microbial and geochemical processes. The integration of biological, geochemical, and geophysical investigations may aid in understanding geophysical responses at LNAPL contaminated sites. Finally, a mechanistic understanding of the processes resulting in the measured geophysical responses remains uncertain and there are no petrophysical or numerical models that incorporate microbial effects. This also presents potential areas for future research.

Acknowledgments We acknowledge the many collaborators (A. Endres, S. Rossbach, W. Sauck, L. Slater) and former students (G. Abdel Aal, J. Allen, V. Che-Alota, C. Davis, J. Duris, F. Legall, D. Werkema) who helped shape the ideas discussed in this review article. We also acknowledge the different funding agencies (the US National Science Foundation, the Petroleum Research Fund of the American Chemical Scociety, and the US Environmental Protection Agency) for financial support that helped develop biogeophysics. V. Che-Alota helped with the literature review and C. Davis provided Fig. 6. Critical reviews from two anonymous reviewers helped to improve this manusucript substantially.

References

Abdel Aal G, Atekwana EA, Slater LD (2004) Effects of microbial processes on electrolytic and interfacial electrical properties of unconsolidated sediments. Geophys Res Lett 31:L12505

Abdel Aal GZ, Slater LD, Atekwana EA (2006) Induced-polarization measurements on unconsolidated sediments from a site of active hydrocarbon biodegradation. Geophysics 71:H13–H24

Abdel Aal G, Atekwana E, Radzikowski S, Rossbach S (2009) Effect of bacterial adsortion on low frequency electrical properties of clean quartz sands and iron-oxide coated sands. Geophys Res Lett 36:L04403. doi:10.1029/2008GL036196

Allen JP, Atekwana EA, Atekwana EA, Duris JW, Werkema DD, Rossbach S (2007) The microbial community structure in petroleum-contaminated sediments corresponds to geophysical signatures. Appl Environ Microbiol 73:2860–2870

Archie GE (1942) The electrical resistivity log as an aid in determining some reservoir characteristics. Trans Am Inst Min Metall Petrol Eng 146:54–61

Atekwana EA, Sauck WA, Werkema DD (2000) Investigations of geoelectrical signatures at a hydrocarbon contaminated site. J Appl Geophys 44:167–180

Atekwana EA, Sauck WA, Abdel Aal GZ, Werkema DD (2002) Geophysical investigation of vadose zone conductivity anomalies at a hydrocarbon contaminated site: implications for the assessment of intrinsic bioremediation. J Environ Eng Geophys 7:103–110

Atekwana EA, Atekwana EA, Werkema DD, Duris JW, Rossbach S, Sauck WA, Cassidy DP, Means J, Legall FD (2004a) In situ apparent conductivity measurements and microbial population distribution at a hydrocarbon-contaminated site. Geophysics 69:56–63

Atekwana EA, Atekwana EA, Rowe RS, Werkema DD, Legall FD (2004b) The relationship of total dissolved solids measurements to bulk electrical conductivity in an aquifer contaminated with hydrocarbon. J Appl Geophys 56:281–294

Atekwana EA, Atekwana E, Legall FD, Krishnamurthy RV (2004c) Field evidence for geophysical detection of subsurface zones of enhanced microbial activity. Geophys Res Lett 31:L23603

Atekwana EA, Atekwana EA, Werkema DD, Allen JP, Smart LA, Duris JW, Cassidy DP, Sauck WA, Rossbach S (2004d) Evidence for microbial enhanced electrical conductivity in hydrocarbon-contaminated sediments. Geophys Res Lett 31:L23501

Atekwana EA, Atekwana EA, Legall FD, Krishnamurthy RV (2005) Biodegradation and mineral weathering controls on bulk electrical conductivity in a shallow hydrocarbon contaminated aquifer. J Contam Hydrol 80:149–167

Atekwana EA, Werkema DD, Atekwana EA (2006) Biogeophysics: the effects of microbial processes on geophysical properties of the shallow subsurface. Appl Hydrogeophys 71:161–193

Benson AK, Stubben MA (1995) Interval resistivities and very low frequency electromagnetic induction—an aid to detecting groundwater contamination in space and time; a case study. Environ Geosci 2:74–84

Benson AK, Payne KL, Stubben MA (1997) Mapping groundwater contamination using dc resistivity and VLF geophysical methods—a case study. Geophysics 62:80–86

Bermejo JL, Sauck WA, Atekwana EA (1997) Geophysical discovery of a new LNAPL plume at the former Wurtsmith AFB, Oscoda, Michigan. Ground Water Monit Remed 17:131–137

Bigalke J, Grabner EW (1997) The geobattery model: a contribution to large scale electrochemistry. Electrochim Acta 42:3443–3452

Börner FD, Schön JH (1991) A relation between the quadrature component of electrical conductivity and specific surface area. The Log Analyst 32:612–613

Bradford JH (2007) Frequency-dependent attenuation analysis of ground-penetrating radar data. Geophysics 72:J7–J16. doi:10.1190/1.2710183

Brovelli A, Malaguerra F, Barry DA (2009) Bioclogging in porous media: model development and sensitivity to initial conditions. Environ Model Softw 24:611–626

Cagniard L (1953) Basic theory of the magneto-telluric method of geophysical prospecting. Geophysics 18(605):605–635

Campbell DL, Lucius JE, Ellefsen KJ, Deszcz-Pan M (1996) Monitoring of a controlled LNAPL spill using ground penetrating radar. In: Proceedings of the symposium on the application of geophysics to engineering and environmental problems (SAGEEP), Keystone, CO, pp 511–517

Carlut J, Horen H, Janots D (2007) Impact of micro-organisms activity on the natural remanent magnetization of the young oceanic crust. Earth Planet Sci Lett 253:497–506

Cassidy NJ (2007) Evaluating LNAPL contamination using GPR signal attenuation analysis and dielectric property measurements: practical implications for hydrological studies. J Contam Hydrol 94:49–75

Cassidy NJ (2008) GPR attenuation and scattering in a mature hydrocarbon spill: a modeling study. Vadose Zone J 7:140–159

Cassidy DP, Werkema DD, Sauck WA, Atekwana EA, Rossbach S, Duris JW (2001) The effects of LNAPL biodegradation products on electrical conductivity measurements. J Environ Eng Geophys 6:47–52

Chapelle FH, Bradley PM (1997) Alteration of aquifer geochemistry by microorganisms. In: Hurst CJ, Knudsen GR, McInerney MJ, Stetzenbach LD, Walter MV (eds) Manual of environmental microbiology. ASM Press, Washington DC, pp 558–564

Chapelle FH, Haack SK, Adriaens P, Henry MA, Bradley PM (1996) Comparison of E(h) and H-2 measurements for delineating redox processes in a contaminated aquifer. Environ Sci Technol 30: 3565–3569

Che-Alota V, Atekwana EA, Atekwana EA, Sauck WA, Werkema DD (2009) Temporal geophysical signatures due to contaminant mass reduction. Geophysics 74. doi: 10.1190/1.3139769

Corwin RF (1990) The self-potential method for environmental and engineering applications: In: Ward SH (ed) Geotechnical and environmental geophysics, vol 1. Review and tutorial. SEG, Tulsa, pp 127–146

Daniels JJ, Roberts R, Vendl M (1995) Ground-penetrating radar for the detection of liquid contaminants. J Appl Geophys 33:195–207

Davis CA (2009) Investigating the impact of microbial interactions with geologic media on geophysical properties. Unpublished dissertation, Missouri University of Science and Technology

Davis JL, Annan AP (1989) Ground-penetrating radar for high-resolution mapping of soil and rock stratigraphy. Geophys Prospect 37:531–551

Davis CA, Atekwana E, Atekwana E, Slater LD, Rossbach S, Mormile MR (2006) Microbial growth and biofilm formation in geologic media is detected with complex conductivity measurements. Geophys Res Lett 33:L18403

DeRyck SM, Redman JD, Annan AP (1993) Geophysical monitoring of controlled kerosene spill. In: Proceedings of the symposium on the application of geophysics to engineering and environmental problems (SAGEEP), San Diego, pp 5–19

Endres AL, Redman J (1996) Modeling the electrical properties of porous rocks and soils containing immiscible contaminants. J Environ Eng Geophys 0:105–112

Eweis JB, Schroeder ED, Chang DPY, Scow KM (1998) Biodegradation of MTBE in a pilot-scale biofilter. In: Wickramanayake GB, Hinchee RE (eds) Natural attenuation: chlorinated and recalcitrant compounds. Battelle Press, Columbus, pp 341–346

Frohlich RK, Barosh PJ, Boving T (2008) Investigating changes of electrical characteristics of the saturated zone affected by hazardous organic waste. J Appl Geophys 64:25–36
Haack SK, Bekins BA (2000) Microbial populations in contaminant plumes. Hydrogeol J 8:63–76
Hubbard SS, Williams K, Conrad ME, Faybishenko B, Peterson JS, Chen J, Long P, Hazen T (2008) Geophysical monitoring of hydrological and biogeochemical transformations associated with Cr(VI) biostimulation. Environ Sci Technol 42:3757–3765. doi:10.1021/es071702s
Huling SG, Pivetz B, Stransky R (2002) Terminal electron acceptor mass balance: light nonaqueous phase liquids and natural attenuation. J Environ Eng 128:246–252
Knight R (2001) Ground penetrating radar for environmental applications. Annu Rev Earth Planet Sci 29:229–255
Lee JY, Cheon JY, Lee KK, Lee SY, Lee MH (2001) Factors affecting the distribution of hydrocarbon contaminants and hydrogeochemical parameters in a shallow sand aquifer. J Contam Hydrol 50: 139–158
Lesmes DP, Frye KM (2001) Influence of pore fluid chemistry on the complex conductivity and induced polarization responses of Berea sandstone. J Geophys Res Solid Earth 106:4079–4090
Lien BK, Enfield CG (1998) Delineation of subsurface hydrocarbon contaminated distribution using a direct push resistivity method. J Environ Eng Geophys 2–3:173–179
Linde N, Revil A (2007) Inverting self-potential data for redox potentials of contaminant plumes. Geophys Res Lett 34:L14302. doi:10.1029/2007GL030084
Lopes de Castro D, Branco RMGC (2003) 4-D ground penetrating radar monitoring of a hydrocarbon leakage site in Fortaleza (Brazil) during its remediation process: a case history. J Appl Geophys 54:127–144
Lucius J, Olhoeft GR, Hill PL, Duke SK (1992) Properties and hazards of 108 selected substances, 1992 edn. United Staes geological survey open file report 92-527, 560 pp
Marcak H, Golebiowski T (2008) Changes of GPR spectra due to the presence of hydrocarbon contamination in the ground. Acta Geophys 56:485–504
Mazác O, Benes L, Landa I, Maskova A (1990) Determination of the extent of oil contamination in groundwater by geoelectrical methods. In: Ward SH (ed) Geotechnical and environmental geophysics, vol 2. pp 107–112
McGuire JT, Smith EW, Long DT, Hyndman DW, Haack SK, Klug MJ, Velbel MA (2000) Temporal variations in parameters reflecting terminal-electron-accepting processes in an aquifer contaminated with waste fuel and chlorinated solvents. Chem Geol 169:471–485
McNeill JD (1990) Use of electromagnetic methods for groundwater studies. In: Ward SH (ed) Geotechnical and environmental geophysics. SEG, IG#5, pp 191–218
Naudet V, Revil A (2005) A sandbox experiment to investigate bacteria-mediated redox processes on self-potential signals. Geophys Res Lett 32:L11405. doi:10.1029/2005GL022735
Naudet V, Revil A, Bottero JY, Begassat P (2003) Relationship between self-potential (SP) signals and redox conditions in contaminated groundwater. Geophys Res Lett 30:2091. doi:10.1029/2003GL018096
Ntarlagiannis D, Ferguson A (2009) SIP response of artificial biofilms. Geophysics 74:A1–A5
Ntarlagiannis D, Williams KH, Slater L, Hubbard S (2005a) Low-frequency electrical response to microbial induced sulfide precipitation. J Geophys Res Biogeosci 110:L24402
Ntarlagiannis D, Yee N, Slater L (2005b) On the low-frequency electrical polarization of bacterial cells in sands. Geophys Res Lett 32:L24402
Ntarlagiannis D, Atekwana EA, Hill EA, Gorby Y (2007) Microbial nanowires: is the subsurface "hard-wired"? Geophys Res Lett 34:L17305
Nyquist JE, Corry CE (2002) Self-potential: the ugly duckling of environmental geophysics. Lead Edge 21:446–451
Olhoeft GR (1985) Low frequency electrical properties. Geophysics 50:2492–2503
Osella A, de la Vega M, Lascano E (2002) Characterization of a contaminant plume due to a hydrocarbon spill using geoelectrical methods. J Environ Eng Geophys 7:78–87
Personna YR, Ntarlagiannis D, Slater L, Yee N, O'Brien M, Hubbard S (2008) Spectral induced polarization and electrodic potential monitoring of microbially mediated iron sulfide transformations. J Geophys Res Biogeosci 113:G02020
Petterssen JK, Nobes DC (2003) Environmental geophysics at Scott Base: ground penetrating radar and electromagnetic induction as tools for mapping contaminated ground at Antarctic research bases. Cold Reg Sci Technol 37:187–195
Poortinga AT, Bos R, Norde W, Busscher HJ (2002) Electric double layer interactions in bacterial adhesion to surfaces. Surf Sci Rep 47:1–32
Revil A, Glover PWJ (1998) Nature of surface electrical conductivity in natural sands, sandstones, and clays. Geophys Res Lett 25:691–694

Rizzo E, Suski B, Revil A, Straface S, Troisi S (2004) Self-potential signals associated with pumping-tests experiments. J Geophys Res 109:B10203. doi:10.1029/2004JB003049
Sato M, Mooney HM (1960) The electrochemical mechanism of sulfide self potential. Geophysics 25: 226–249
Sauck WA (2000) A model for the resistivity structure of LNAPL plumes and their environs in sandy sediments. J Appl Geophys 44:151–165
Sauck WA, Atekwana EA, Nash MS (1998) High conductivities associated with an LNAPL plume imaged by integrated geophysical techniques. J Environ Eng Geophys 2:203–212
Saul DJ, Aislabie JM, Brown CE, Harris L, Foght JM (2005) Hydrocarbon contamination changes the bacterial diversity of soil from around Scott Base, Antarctica. FEMS Microbiol Ecol 53:141–155
Schön JH (1996) Handbook of geophysical exploration, volume 18, physical properties of rocks: fundamentals and principles of petrophysics. Elsevier, Pergamon
Sivenas P, Beales FW (1982) Natural geobatteries associated with sulphide ore deposits, I. Theoretical studies. J Geochem Explor 17:123–143
Skubal KL, Barcelona MJ, Adriaens P (2001) An assessment of natural biotransformation of petroleum hydrocarbons and chlorinated solvents at an aquifer plume transect. J Contam Hydrol 49:151–169
Slater LD, Glaser DR (2003) Controls on induced polarization in sandy unconsolidated sediments and application to aquifer characterization. Geophysics 68:1547–1558
Slater LD, Lesmes D (2002) IP interpretation in environmental investigations. Geophysics 67:77–88
Slater L, Ntarlagiannis D, Personna YR, Hubbard S (2007) Pore-scale spectral induced polarization signatures associated with FeS biomineral transformations. Geophys Res Lett 34:L21404
Sogade JA, Scira-Scappuzzo F, Vichabian Y, Shi WQ, Rodi W, Lesmes DP, Morgan FD (2006) Induced-polarization detection and mapping of contaminant plumes. Geophysics 71:B75–B84
Stoll J, Bigalke J, Grabner EW (1995) Electrochemical modeling of self-potential anomalies. Surv Geophys 16:107–120
Tezkan B, Georgescu P, Fauzi U (2005) A radiomagnetotelluric survey on an oil-contaminated area near the Brazi Refinery, Romania. Geophys Prospect 53:311–323
Vandevivere P, Baveye P (1992) Effect of bacterial extracellular polymers on the saturated hydraulic conductivity of sand columns. Appl Environ Microbiol 58:1690–1698
Vroblesky DA, Chapelle FH (1994) Temporal and spatial changes of terminal electron-accepting processess in a petroleum hydrocarbon-contaminated aquifer and the significance for contaminant biodegradation. Water Resour Res 30:1561–1570
Waxman MH, Smits LJM (1968) Electrical conductivities in oil-baring shaly sands. Soc Petrol Eng J 8: 107–122
Werkema DD, Atekwana EA, Endres AL, Sauck WA, Cassidy DP (2003) Investigating the geoelectrical response of hydrocarbon contamination undergoing biodegradation. Geophys Res Lett 30:1647. doi: 10.1029/2003GL017346
Williams KH, Ntarlagiannis D, Slater LD, Dohnalkova A, Hubbard SS, Banfield JF (2005) Geophysical imaging of stimulated microbial biomineralization. Environ Sci Technol 39:7592–7600
Williams KH, Hubbard SS, Banfield JF (2007) Galvanic interpretation of self-potential signals associated with microbial sulfate-reduction. J Geophys Res Biogeosci 112:G03019
Yang CH, Yu CY, Su SW (2007) High resistivities associated with a newly formed LNAPL plume imaged by geoelectric techniques—a case study. J Chin Inst Eng 30:53–62